Acta Geodyn. Geomater., Vol. 23, No. 3 (223), 371–392, 2026
DOI: 10.13168/AGG.2026.0025
journal homepage: https://www.irsm.cas.cz/acta

ORIGINAL PAPER

GRAIN BREAKAGE–INDUCED EVOLUTION OF GRAIN SIZE DISTRIBUTION, PORE STRUCTURE, AND PERMEABILITY OF SANDS UNDER HIGH OEDOMETRIC STRESS

Sadok FEIA [1)], Abdelali DADDA [2, 3)], *, Seyf Eddine MESSIOUD [1, 3)], Wang JIPENG [2)] and Li NAN [2)]

[1)] *Civil Engineering Research Laboratory, Biskra University, 07000, Biskra, Algeria.*
[2)] *School of Civil Engineering, Shandong University, 17922 Jingshi Road, Jinan 250061, China*
[3)] *SMARTSKY Engineering, Algiers, Algeria*

**Corresponding author's e-mail:* abdelali.dadda@sdu.edu.cn

ARTICLE INFO

Article history:
Received 7 August 2025
Accepted 22 June 2026
Available online 2 September 2026

Keywords:
Grain breakage
Permeability
Pore structure
Oedometric behavior
Granular materials

ABSTRACT

Grain breakage under high stress conditions can significantly affect the hydro-mechanical behavior of granular materials by altering grain size distribution, pore structure, porosity, and permeability. This study investigates these coupled effects in two sands with contrasting mineralogical characteristics, namely Hostun silica sand and carbonate sand, subjected to high oedometric stresses up to 105 MPa. High-pressure oedometer tests were performed on dense specimens prepared at a relative density of approximately 0.9. Grain size distribution was determined by post-loading sieve analysis, while permeability was measured at different stress levels using a constant-head system connected to the oedometer cell. Pore-access size distribution was characterized using two complementary techniques depending on material response and stress level: the tensiometric method, based on drying-path water retention measurements and the Young–Laplace law, and mercury intrusion porosimetry for carbonate sand specimens that developed sufficient cohesion after high-stress loading. The results show that increasing stress induces progressive grain fragmentation, leading to an evolution of the grain size distribution toward an ultimate grading state, together with reductions in pore size and porosity. The crushing threshold was identified at approximately 12.5 MPa for Hostun sand and 3 MPa for carbonate sand, indicating the strong influence of mineralogical composition on breakage resistance. Permeability decreased markedly with stress, with a reduction of about 50 % for Hostun sand and more than 70 % for carbonate sand. This stronger reduction in carbonate sand is associated with more pronounced particle breakage, pore structure modification, fines production, and reduced pore connectivity. The experimental results were interpreted using the Continuum Breakage Mechanics framework, and a power-law relationship between permeability and porosity was calibrated for both sands. The analysis indicates that grain rearrangement and grain breakage jointly control porosity and permeability reduction, with the influence of grain breakage becoming increasingly significant at higher stress levels, particularly for carbonate sand.These findings provide an experimental and modeling basis for understanding the coupled effects of high stress, grain breakage, pore structure evolution, and permeability reduction in sands, with implications for geotechnical, geomechanical, and petroleum reservoir engineering applications.

1. INTRODUCTION

Particle breakage in granular soils is a recurrent phenomenon in various geotechnical and geomechanical contexts. It occurs notably under the high stress levels near pile foundations (Zhang et al., 2013; Altuhafi et al., 2017), within shear zones of landslides (Wang et al., 2002; Igwe et al., 2007), and in petroleum reservoirs, where high-pressure water injection for oil production or enhanced recovery generates significant mechanical loading (Feia et al., 2016, 2017). This process induces microstructural transformations, affecting interparticle forces, altering grain morphology, and modifying particle size distribution (Karatza et al., 2017, 2018, 2019). These changes directly influence the hydro-mechanical behavior of granular soils, impacting strength, deformation, and permeability (Feia et al., 2016; Chen et al., 2018). A thorough understanding of this phenomenon is therefore of strategic importance, particularly in petroleum engineering, where it contributes to optimizing hydrocarbon recovery strategies while reducing operational costs.

Grain breakage affects both the microstructural integrity and the macroscopic mechanical behavior of granular materials. When the contact forces transmitted through the granular assembly exceed the strength of individual grains, fragmentation occurs, leading to a progressive modification of the grain size distribution. Fredlund et al. (2011) demonstrated that changes in granulometry can be used to estimate the soil-water characteristic curve, thereby linking particle size distribution to hydraulic behavior. Al-Hattamleh et al. (2013) further showed that crushing can reduce permeability, emphasizing the hydraulic consequences of particle degradation. This phenomenon has been investigated for several

Cite this article as: Feia S, Dadda A, Messioud SE, Jipeng W, Nan L: Grain breakage–induced evolution of grain size distribution, pore structure, and permeability of sands under high oedometric stress. Acta Geodyn. Geomater., 23, No. 3 (223), 371–392, 2026. DOI: 10.13168/AGG.2026.0025

decades, with major contributions from Turcotte (1986), Fukumoto (1990, 1992), Fredlund et al. (2000), Coop et al. (2004), and Al-Hattamleh et al. (2013), who collectively advanced the understanding of fragmentation mechanisms and their mechanical and hydraulic implications.

Particle breakage generates finer fragments that progressively occupy the voids between larger grains, thereby modifying packing density and soil fabric (Zhao et al., 2019; Messioud et al., 2024). Lee and Farhoomand (1967) related crushing-induced changes in grain size distribution to compressibility, while Hardin's relative breakage index (B_r) (Hardin, 1985) provided a robust and reproducible metric for quantifying particle degradation and its mechanical consequences. Einav's continuum breakage mechanics (CBM) framework (Einav, 2007a, 2007b) further incorporated grain size distribution evolution and particle shape into constitutive modelling through fractal size distributions and morphology-dependent energy dissipation.

Recent advances have extended these theoretical frameworks. Zhang et al. (2021) proposed an elastoplastic model for gravelly soils that couples void ratio, particle breakage, and dilatancy. Tong et al. (2019) incorporated the evolution of coordination number into a stochastic breakage model under compression, demonstrating how changes in the contact network control gradation evolution. Yao et al. (2025) developed a predictive model based on grain size distribution evolution, deriving fractal scaling laws and energy dissipation coefficients across multiple size fractions. Taken together, these studies have significantly improved the ability to describe how particle size and morphology govern fabric evolution and macroscopic mechanical behavior.

The resistance of granular materials to breakage depends on both intrinsic grain properties and environmental conditions. Mineralogical composition controls brittleness and fracture toughness; for example, carbonate sands are more prone to breakage under comparable stress paths because of their lower hardness and the presence of pre-existing flaws (Coop et al., 2004). Grain size distribution also influences stress partitioning within the granular assembly. Well-graded materials can redistribute stresses through finer particles, thereby delaying fragmentation, whereas uniform or gap-graded fabrics tend to concentrate loads and accelerate crushing (Nakata et al., 2001). Grain morphology, particularly angularity, amplifies local stress concentrations by reducing contact area and promoting micro-crack initiation (Marachi, 1969). Moisture content may also affect breakage behavior: low saturation can enhance interparticle bonding through capillary forces and delay crushing, whereas high saturation, together with reduced effective stress, may promote fracture under high confining pressure. However, this response depends strongly on mineralogy, density, and stress path (Yamamuro and Lade, 1996; Asaf et al., 2007; Frossard et al., 2012; Han et al., 2016). X-ray micro-tomography has further shown that fragmentation is often localized within shear bands, where it evolves through a feedback mechanism between strain localization and particle breakage (Karatza et al., 2018).

Particle breakage reorganizes the granular skeleton and progressively reduces porosity as applied stress increases (Chuhan, 2002). The resulting changes in pore structure, including pore size distribution and tortuosity, have a strong influence on permeability and elastic modulus (Burdine, 1953; Juang and Holtz, 1986; Aung et al., 2001; Benammar et al., 2025). Pore size distribution can be characterized using mercury intrusion porosimetry (MIP), capillary condensation, and tensiometric methods. MIP enables the characterization of a broad pore-size range and provides information on porosity and pore connectivity (Katz and Thompson, 1986). Capillary condensation, based on the Kelvin–Young–Laplace relation, is widely used to characterize smaller pores (Charlaix and Ciccotti, 2009). The tensiometric method, which is particularly suitable for cohesionless materials, derives pore access size from the soil-water retention curve using the Young–Laplace law (Feia et al., 2014), offering valuable insight into pore-structure evolution and its effect on permeability.

The critical state framework for sands incorporating particle breakage has been progressively refined through experimental and analytical investigations. Previous studies have demonstrated a complex coupling between particle breakage and macroscopic behavior under high stress, where changes in particle size and morphology influence both compressibility and strength (Tengattini et al., 2016; Chen et al., 2023). Recent constitutive models now couple brittle grain mechanics with the coevolution of grain size and shape, improving predictions under various loading paths (Buscarnera and Einav, 2021). In addition, recent studies quantifying particle shape evolution during crushing through imaging techniques, single-particle tests, and DEM/FDEM simulations confirm that morphological changes, in addition to size reduction, significantly affect deformation and strength at the assembly scale. These findings strongly support the incorporation of particle shape evolution into modern constitutive models (Xiao, 2022; Dong et al., 2024).

Although significant progress has been made in modeling granular materials, the coupling between grain breakage, pore structure evolution, and permeability remains insufficiently documented under high oedometric stress conditions. In particular, the experimental validation of breakage-related parameters, such as the crushing threshold and its influence on hydraulic behavior, is still limited. Furthermore, the respective contributions of grain rearrangement and grain breakage to changes in porosity and permeability are not yet fully understood, especially for sands with contrasting mineralogical properties.

In this context, the present study aims to investigate the coupled effects of grain breakage on the mechanical behavior, grain size distribution, pore-access size distribution, and permeability of sands subjected to high oedometric stresses. An experimental program was conducted on two sands with distinct mineralogical properties, namely Hostun silica sand and carbonate sand.

High-pressure oedometer tests were performed up to 105 MPa, combined with permeability measurements at different loading stages using a constant-head system. Grain size distribution evolution was quantified through post-test sieve analyses. Pore-access size distribution was characterized using two complementary methods: the tensiometric approach, based on water retention curves and the Young–Laplace law, and mercury intrusion porosimetry for high-stress conditions where sufficient cohesion was developed.

The results are interpreted within the framework of Continuum Breakage Mechanics (CBM) to identify the crushing threshold and quantify grain breakage. In addition, a power-law relationship between permeability and porosity is calibrated to assess the impact of pore structure changes on hydraulic behavior. These experimental results also provide indirect support for the breakage framework proposed by Einav (2007a, 2007b).

This study provides a comparative analysis of silica and carbonate sands and offers new experimental insights into the coupling between grain breakage, pore structure evolution, and permeability under high stress conditions, contributing to improved predictive modeling in geotechnical, geomechanical, and petroleum reservoir engineering applications.

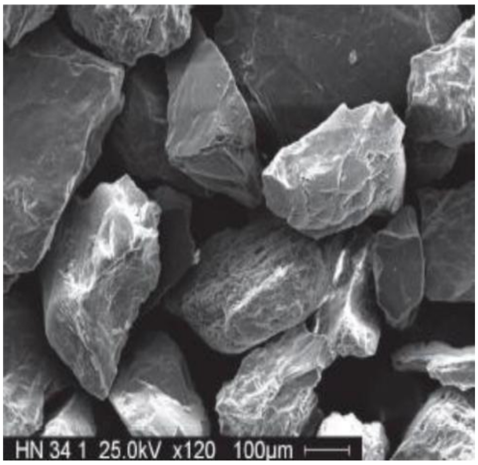

(a)

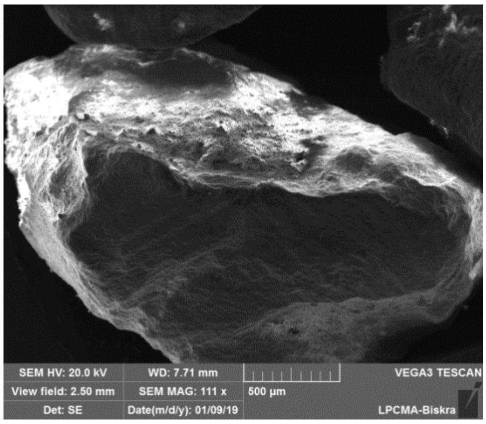

(b)

Fig. 1 Scanning electron microscope for used sands; (a) Hostun sand, (b) Carbonate sand.

2. MATERIALS AND METHODS

2.1. MATERIALS

Two sands with distinct mineralogical compositions were investigated, namely Hostun sand and carbonate sand.

Hostun sand (HN34) is a clean, poorly graded silica sand composed of sub-angular grains, as illustrated in Figure 1a. Its particle size distribution is presented in Figure 2a.

In contrast, the carbonate sand is a well-graded material predominantly composed of calcite ($CaCO_3$), representing approximately 98 % of its mass, and derived mainly from biogenic sources such as coral fragments, mollusk shells, and calcareous algae. Scanning Electron Microscopy (SEM) observations (Fig. 1b) reveal that the grains exhibit an angular morphology with highly irregular surfaces and pronounced micro-scale asperities. This intrinsic surface roughness is expected to significantly influence interparticle contact interactions and, consequently, the macroscopic mechanical behavior of the material. Its grain size distribution is also shown in Figure 2a.

The main physical characteristics of both sands are summarized in Table 1, including the median grain size (D_{50}), the uniformity coefficient ($C_U = D_{60}/D_{10}$), and the grain density (ρ_s). Hostun sand exhibits a finer and more uniform grading (D_{50} = 0.207 mm, C_U = 1.57), whereas carbonate sand is coarser and more broadly graded (D_{50} = 0.629 mm, C_U = 7.67).

These differences in grain size distribution and grading significantly influence the pore-access size distribution, as shown in Figure 2b. The pore size distributions were derived from drying-path water retention curves for specimens prepared at a relative density of approximately 0.9, following the methodology proposed by Feia et al. (2014).

Under identical initial density conditions, the carbonate sand exhibits smaller pore-access sizes compared to Hostun sand. This behavior is primarily attributed to its well-graded structure, which promotes a denser packing and finer pore network, whereas the poorly graded Hostun sand results in a coarser pore structure. These initial differences play an important role in the subsequent mechanical and hydraulic response of the two materials.

(a)

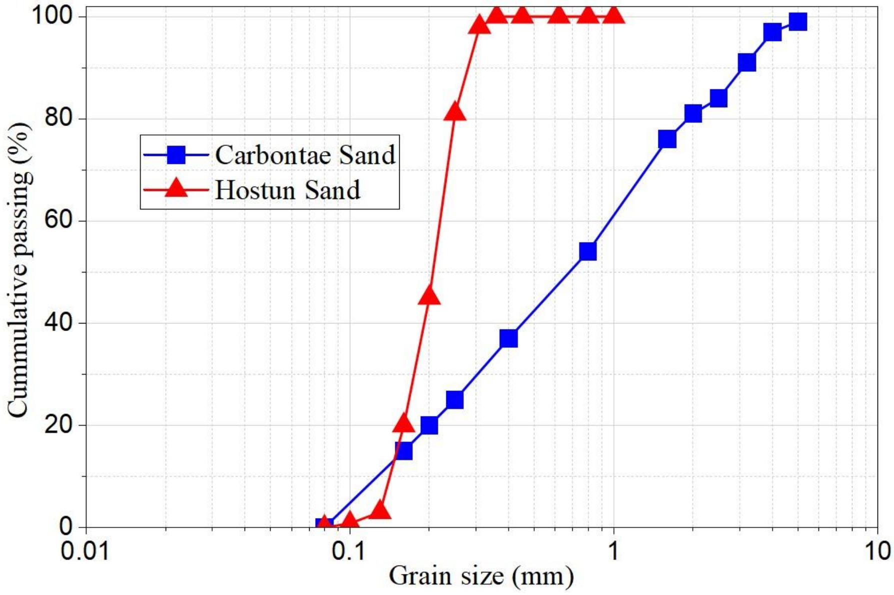

(b)

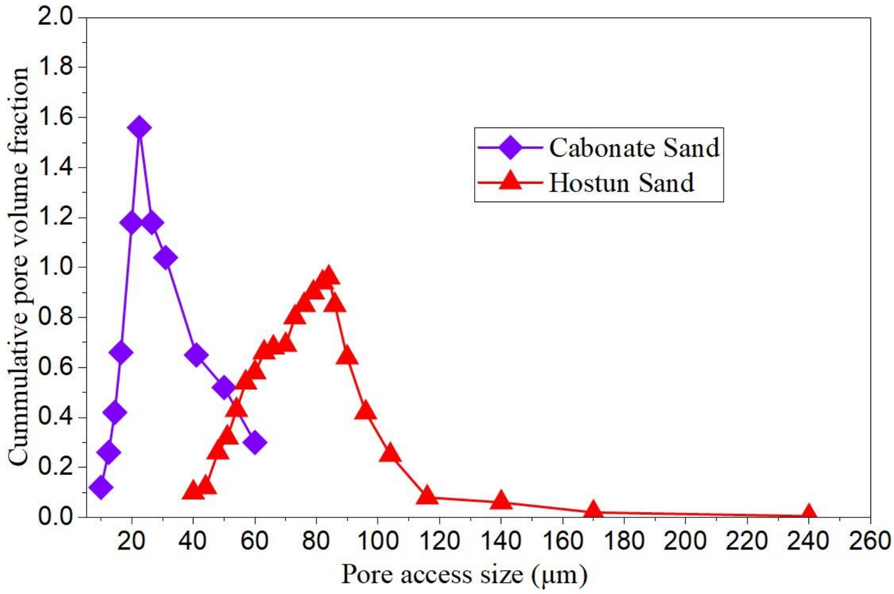

Fig. 2 Initial characteristics, (a) Grain size distribution, (b) Pore size distribution.

Table 1 Characteristics of the tested sands.

Sand	D_{50} (mm)	C_U	e_{min}	e_{min}	ρ_s (g/cm^3)
Hostun sand (HN34)	0.207	1.57	0.696	1.145	2.65
Carbonate sand	0.629	7.67	0.33	0.59	2.65

2.2. EXPERIMENTAL SETUP

2.2.1. OEDOMETER TESTING PROCEDURE

High-pressure oedometer tests were conducted using a device capable of applying vertical stresses up to approximately 113 MPa on cylindrical specimens with a diameter of 38 mm (Marcial et al., 2002). Figure 3 illustrates the schematic configuration of the high-pressure oedometer apparatus.

The experiments were performed on dense samples prepared with a controlled relative density of approximately 0.9. Specimens with diameters of 38 mm and 50 mm and a height of 37 mm were used for both sands. A series of increasing stress levels (8, 15, 30, 50, 80, and 105 MPa) was applied.

To investigate the evolution of mechanical behavior associated with grain breakage, both loading and unloading cycles were performed at each stress level. The detailed test conditions and corresponding specimen characteristics are summarized in Table 2.

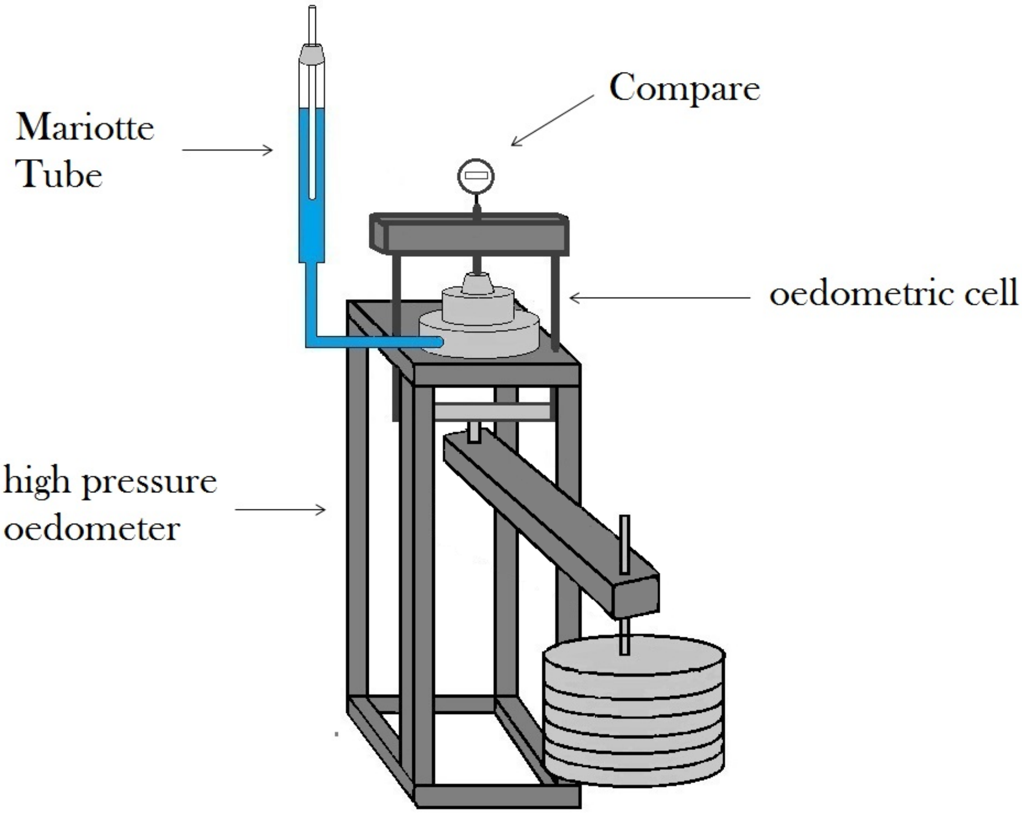

Fig. 3 Schematic presentation of the used device.

Table 2 Tests Conditions and characteristics.

Maximal stress (MPa)	Hostun sand (HN34)				Carbonate sand			
	Static test		Cyclic test		Static test		Cyclic test	
	I_D	Porosity (%)	I_D	Porosity (%)	I_D	Porosity (%)	I_D	Porosity (%)
8	0.89	26.30	0.90	24.09	0.9	42.55	0.86	43.12
15	0.91	26.10			0.89	42.70		
30	0.89	26.39			0.91	42.40		
50	0.90	26.25			0.86	43.14		
80	0.88	26.45			0.87	42.99		
105	0.90	26.18			0.90	42.55		

2.2.2. PERMEABILITY MEASUREMENT

Permeability was measured at each loading stage using a constant-head system based on a Mariotte tube connected to the drainage system of the oedometer cell, as illustrated in Figure 3. This configuration ensures a stable hydraulic gradient throughout the test.

After each test, the grain size distribution of the specimens was determined through sieve analysis in order to quantify the changes induced by loading and grain breakage.

2.2.3. PORE-ACCESS SIZE DISTRIBUTION MEASUREMENT

The pore-access size distribution was determined using two complementary experimental methods, namely the tensiometric method and mercury intrusion porosimetry (MIP), depending on the stress level and the mechanical state of the tested material.

The tensiometric method was used to evaluate pore-access size distribution from drying-path water retention measurements, following the methodology proposed by Feia et al. (2014). The experimental setup consisted of an oedometer cell equipped with a saturated ceramic porous stone connected to a graduated water tube and a de-aired water reservoir, ensuring hydraulic continuity during testing. The measurement setup is schematized in the study of Feia et al. (2014), as illustrated in Figure 4.

In this approach, suction was progressively increased within the specimen, and the corresponding variations in water content were measured after hydraulic equilibrium was reached. The pore-access diameter associated with each suction level was determined using the Young–Laplace equation:

$$s = u_a - u_w = \frac{4\sigma_S cos\theta}{d_p} \quad (1)$$

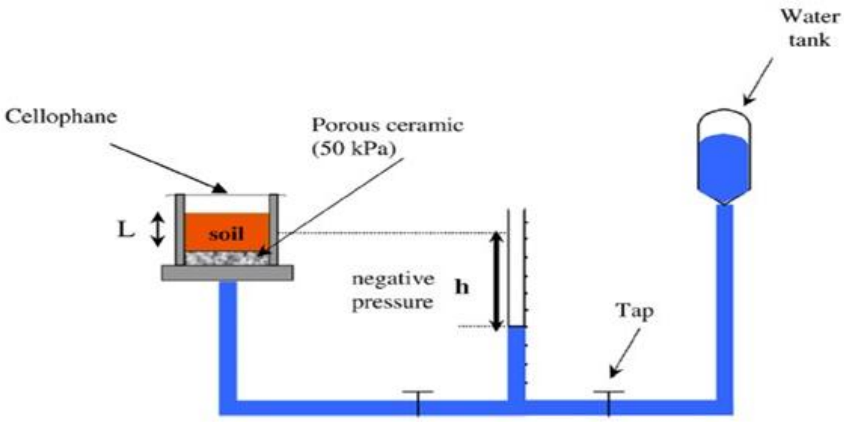

Fig. 4 Schematic representation of the tensiometric setup used for suction measurement (Feia et al., 2014).

Where s is the suction, u_a and u_w are the air and water pressures, respectively, d_p is the pore-access diameter, σ_s is the surface tension of the air–water interface, and θ is the contact angle between the fluid and the solid surface. For granular materials, $cos\theta \approx 1$ is commonly assumed. The pore-access size distribution is then derived from the drying branch of the water retention curve.

However, this method requires a continuous hydraulic connection through the ceramic porous stone, which has limited mechanical resistance. In the present study, this limitation restricts the applicability of the tensiometric method to relatively low stress levels. Consequently, it was applied only at 5 MPa for Hostun sand.

To extend the characterization to higher stress levels, mercury intrusion porosimetry (MIP) was employed for carbonate sand specimens after high-stress loading. This technique is based on the non-wetting behavior of mercury, which requires the application of external pressure to intrude mercury into the pore network. The relationship between the applied pressure and the pore-access diameter is given by:

$$P = \frac{4\sigma_{Hg} cos\theta}{d_p} \quad (2)$$

where P is the applied pressure, σ_{Hg} is the surface tension of mercury, θ is the contact angle between mercury and the pore wall (typically about 140°), and dp is the pore-access diameter. In practice, a dried specimen is subjected to increasing pressure under vacuum, and the intruded mercury volume is measured at each step, allowing the determination of pore volume and pore size distribution.

In the present study, MIP was applied only to carbonate sand specimens, as these developed sufficient cohesion after high-stress loading to preserve their structure during testing. In contrast, Hostun sand remained non-cohesive even after loading and could not be reliably tested using this technique. Consequently, pore-access size distribution for Hostun sand was evaluated only using the tensiometric method at low stress levels.

3. EXPERIMENTAL RESULTS

3.1. MECHANICAL RESPONSE

3.1.1. STRESS–STRAIN RESPONSE AND IDENTIFICATION OF THE CRUSHING THRESHOLD

The compressibility response of granular materials subjected to high stress levels generally exhibits a change in slope that is commonly associated with the onset of particle breakage. Following Biarez and Hicher (1994) and Novello and Johnston (1989), this transition may be interpreted as a crushing threshold, which corresponds to the onset of particle breakage, analogous to the preconsolidation stress in classical soil mechanics. In the present study, the mechanical response was analyzed from the axial strain–applied stress curves obtained during high-pressure oedometric loading, as shown in Figure 5.

For both sands, the strain–stress curves exhibit a nonlinear compressive response characterized by a progressive change in curvature. At low stress levels, deformation is primarily governed by grain rearrangement, pore collapse, and interparticle contact deformation. As the applied stress increases, a distinct change in slope is observed, indicating a transition toward a regime where particle breakage becomes progressively significant. As illustrated in Figure 5, the identified crushing thresholds correspond to the onset of particle breakage for both materials, marked by a clear change in the slope of the curves. This transition reflects a shift from a rearrangement-dominated regime to a breakage-influenced mechanical response.

The crushing threshold is approximately 12.5 MPa for Hostun sand (HN34) and about 3 MPa for carbonate sand. This significant difference highlights the influence of mineralogical composition on breakage resistance. Carbonate sand exhibits a much lower resistance to particle breakage due to its weaker structure, whereas silica-based Hostun sand

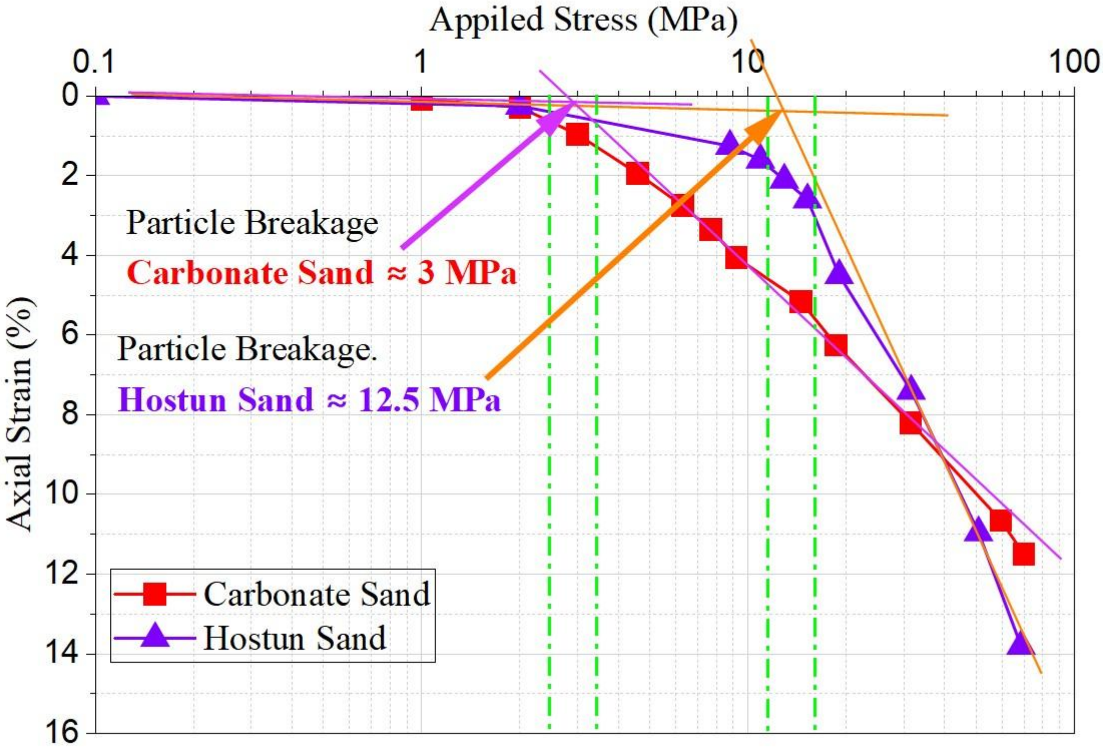

Fig. 5 Strain-stress curves for the two sands.

shows higher resistance and a delayed transition toward grain-crushing-dominated behavior.

The mechanical response of both sands can be interpreted in terms of three distinct deformation phases, each characterized by specific mechanisms associated with the evolution of the applied stress.

In the first phase, corresponding to the initial loading stage, the strain–stress curves of both materials exhibit a quasi-linear behavior with a relatively low slope. This regime is primarily governed by particle rearrangement, pore collapse, and interparticle contact deformation, with no significant grain breakage. At this stage, the void ratio remains relatively high, and the granular structure is preserved, as particles remain largely intact. Both materials therefore exhibit a relatively compliant mechanical response under increasing stress.

The second phase begins near the crushing threshold, which differs for the two sands, occurring at approximately 3 MPa for carbonate sand and 12.5 MPa for Hostun sand. At these stress levels, a noticeable change in the slope of the curves is observed, corresponding to the onset of particle breakage. Grain crushing initiates, and plastic deformation becomes more pronounced. The mechanical response progressively deviates from the initial regime, reflecting the increasing contribution of particle breakage to the overall deformation. This stage marks a fundamental transition in the governing mechanisms, from a rearrangement-dominated regime to a breakage-influenced mechanical response.

In the third phase, at higher stress levels, the compressibility curve exhibits a much steeper slope, indicating a significant increase in compressibility. This regime is characterized by intense particle fragmentation and the generation of finer particles, which progressively fill the pore space and lead to a substantial reduction in void ratio. The continued breakage and redistribution of particles result in a denser and more stable granular structure.

This evolution is consistent with the interpretation proposed by McDowell (2002), who described the progressive transition of granular materials toward a more rock-like behavior under high stress conditions. As the applied stress increases, larger particles become shielded by the surrounding finer fragments, reducing tensile stress concentrations and limiting further breakage. At the same time, smaller particles approach their fragmentation limit, leading to a stabilization of the microstructure. This results in an apparent increase in stiffness and marks the transition toward a more rigid and coherent mechanical response.

This interpretation is further supported by recent experimental studies based on high-resolution 3D X-ray tomography (Karatza et al., 2017; Messioud et al., 2024), which provide direct insight into the underlying microstructural mechanisms. These studies demonstrate that the onset of particle breakage coincides with the intersection of the two tangential slopes of the stress–strain curve, confirming the physical significance of the identified crushing threshold. In addition, the 3D imaging results reveal the progressive evolution of pore collapse, particle fragmentation, and the generation of fine particles throughout the loading process. These observations

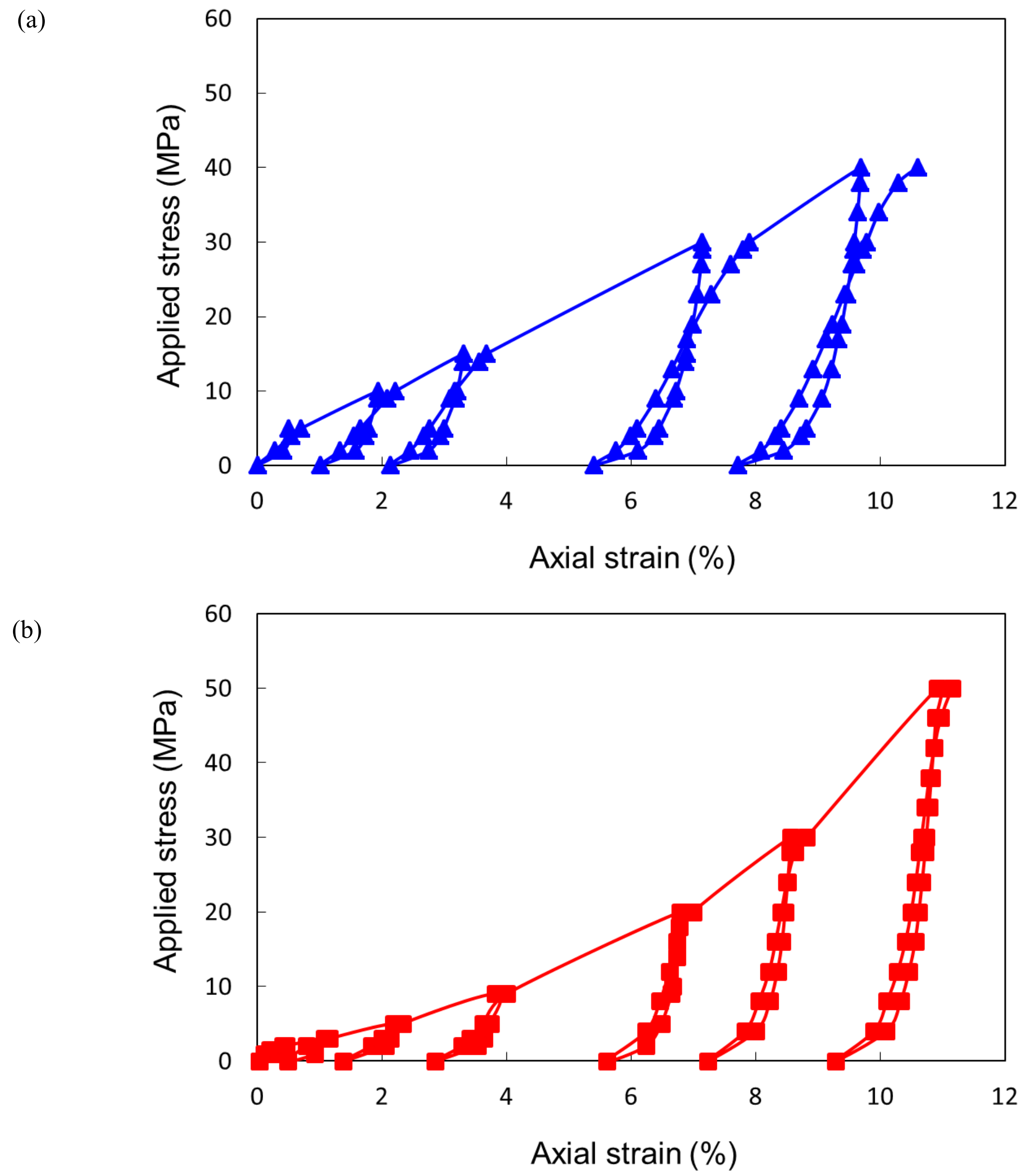

Fig. 6 Loading-unloading curves in oedometer test, (a) Hostun sand, (b) Carbonate sand.

clearly illustrate the transition in material behavior, highlighting how the granular assembly evolves from a loose structure toward a denser and more stable configuration under increasing stress.

This interpretation is further supported by the compression indices obtained from the two portions of the curves. For Hostun sand, the compression indices are $C_{c1} = 1.56 \times 10^{-3}$ and $C_{c2} = 1.95 \times 10^{-3}$, whereas for carbonate sand they are $C_{c1} = 2 \times 10^{-3}$ and $C_{c2} = 2 \times 10^{-3}$. In both cases, the higher value of the second compression index confirms that the material becomes more compressible after the onset of particle breakage. The more pronounced increase observed for carbonate sand further highlights the dominant role of grain breakage in its deformation behavior.

3.1.2. EVOLUTION OF THE OEDOMETRIC MODULUS AND ITS RELATION TO PARTICLE BREAKAGE

To further investigate the evolution of mechanical stiffness, loading–unloading cycles were performed at different stress levels for both sands (Fig. 6). The unloading–reloading curves become progressively steeper with increasing applied stress, indicating a continuous increase in the oedometric modulus as the material densifies under loading.

The evolution of the oedometric modulus is presented in Figure 7. For both sands, the modulus increases approximately linearly with applied stress. This behavior reflects the progressive stiffening of the granular assembly, primarily governed by densification through particle rearrangement, reduction of void space, and gradual reorganization of the internal structure.

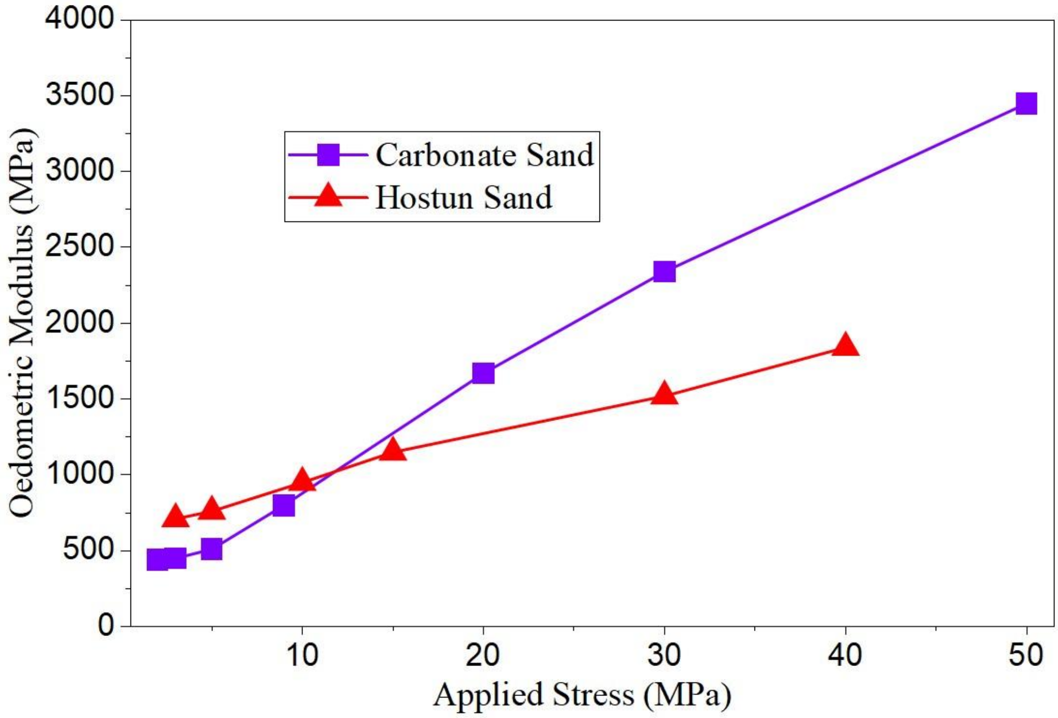

Fig. 7 Evolution of oedometric modulus for both sands.

As stress increases, the evolution of the oedometric modulus reflects not only densification due to particle rearrangement but also the progressive modification of the granular structure associated with grain breakage. The generation of finer particles leads to a reduction in pore space, promotes a denser packing configuration, and increases the number of interparticle contacts. This microstructural reorganization enhances load transfer within the granular assembly and contributes to the observed increase in stiffness.

Such mechanisms have been clearly evidenced in previous studies using high-resolution 3D X-ray tomography (Karatza et al., 2017; Zhao et al., 2019; Messioud et al., 2024), which provide both qualitative and quantitative observations of particle fragmentation, pore space reduction, and the evolution of contact networks under increasing stress. These findings support the interpretation adopted in the present study and confirm that the increase in oedometric modulus reflects the combined effects of densification and structural reorganization induced by grain breakage.

In this context, the oedometric modulus should be regarded as a complementary mechanical parameter that captures the global stiffening and structural evolution of the material during loading. It reflects the combined effects of densification and grain breakage, without being used as a direct indicator of the onset of particle crushing. The identification of particle breakage remains primarily based on the change in slope of the compressibility curve, while the oedometric modulus provides additional insight into the mechanical consequences of the evolving granular structure.

Overall, the results indicate that carbonate sand exhibits a more pronounced increase in oedometric modulus compared to Hostun sand. This behavior is consistent with its higher compressibility, lower resistance to particle breakage, and stronger structural reorganization under oedometric loading. These observations are in agreement with the mineralogical characteristics of carbonate materials and are further supported by the evolution of grain size distribution and pore structure discussed in the following sections.

3.2. EVOLUTION OF THE GRAIN SIZE DISTRIBUTION

Grain breakage directly affects the grain size distribution of granular materials. Accordingly, monitoring the evolution of the grain size distribution (GSD) curve is a widely accepted approach for quantifying particle breakage (Hardin, 1985; Einav, 2007a). In the present study, particle size distribution analyses were performed after the oedometric tests at different stress levels in order to examine the progressive evolution of the GSD with increasing applied stress. The corresponding results for Hostun sand and carbonate sand are presented in Figure 8.

For both sands, the grain size distribution curves shift progressively with increasing stress, indicating continuous particle fragmentation during loading. This evolution is characterized by an increasing proportion of finer particles and a corresponding modification of the grading curves. The shift is more pronounced at intermediate particle sizes, reflecting the progressive breakage of larger grains into smaller fragments.

The evolution of the GSD differs significantly between the two materials. For Hostun sand, the grain size distribution remains relatively close to the initial

(a)

(b)

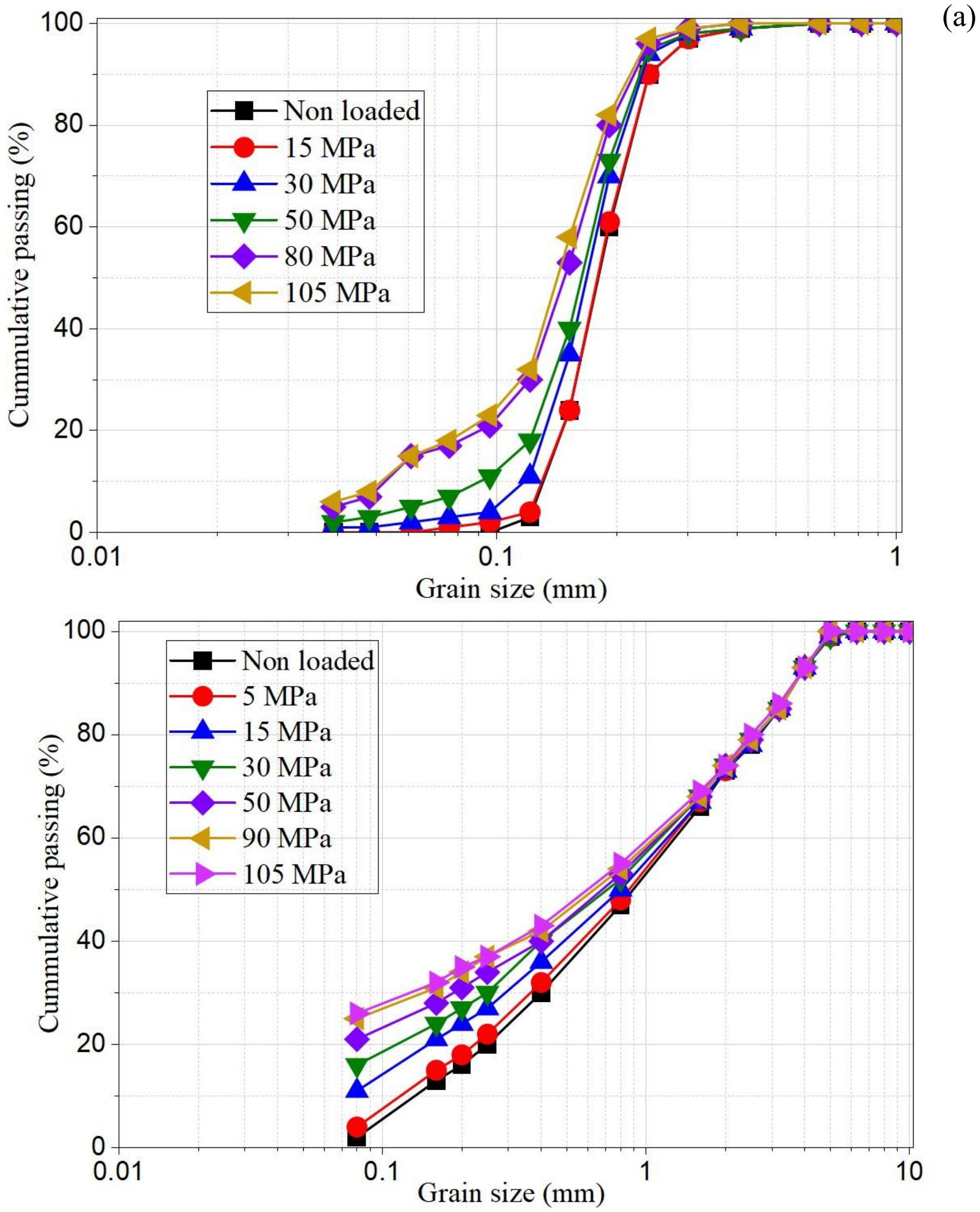

Fig. 8 Evolution of the grain size distribution curves; (a) Hostun sand, (b) Carbonate sand.

curve at low stress levels and evolves progressively as the applied stress increases. This gradual shift reflects a relatively higher resistance to particle breakage. In contrast, the carbonate sand exhibits a more pronounced and earlier modification of its grain size distribution, with a clear increase in fine particles observed from the initial loading stages. This behavior highlights the higher crushability of carbonate sand and its greater sensitivity to stress-induced fragmentation.

Although the evolution of the grain size distribution is significant for both materials, the rate of change decreases progressively as stress increases. The curves tend to approach an ultimate distribution, as suggested by Einav (2007a). This trend indicates that the breakage process evolves toward a limiting state. As fragmentation progresses, the particle assembly becomes more efficiently packed, leading to an increase in the number of interparticle contacts and a more homogeneous distribution of stresses within the granular skeleton. Consequently, stress concentrations on individual grains are reduced, and the material develops an increasing resistance to further breakage.

Recent studies based on high-resolution 3D X-ray tomography (Zhao et al., 2019) further highlight the fundamental role of grain size evolution induced by particle breakage in controlling the overall mechanical behavior of granular materials. These studies demonstrate that the generation of fragments and fine particles of varying sizes and shapes leads to their progressive accumulation around larger grains, resulting in pore clogging and a significant modification of the internal microstructure. This process alters both the interparticle contact force distribution and the pore network geometry, thereby

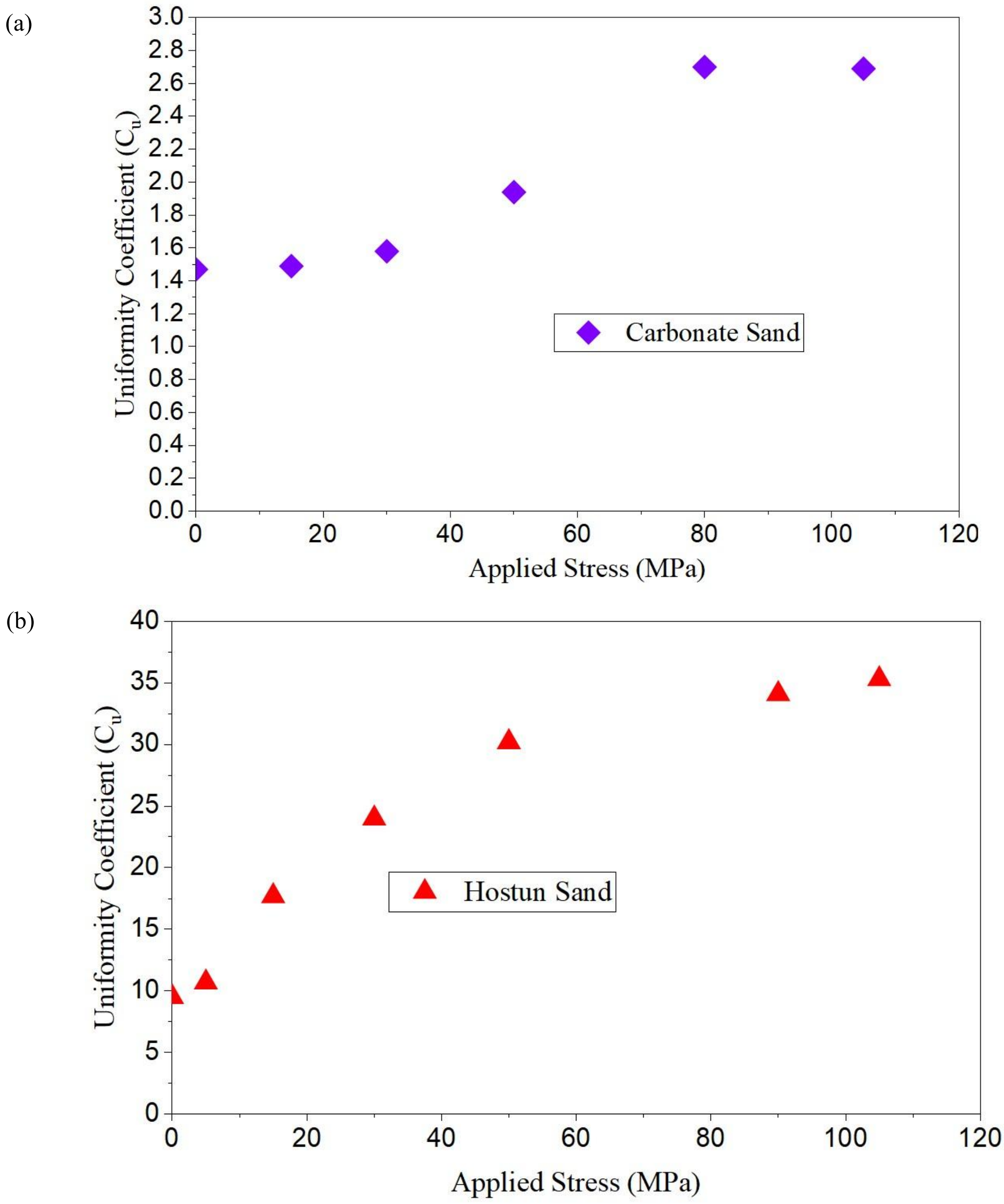

Fig. 9 Evolution of the uniformity coefficient, (a) Hostun sand, (b) Carbonate sand.

directly influencing the macroscopic mechanical response of the material.

To further quantify this evolution, the uniformity coefficient $C_U = D_{60}/D_{10}$ was determined for both sands, where D_{60} and D_{10} correspond to particle diameters at 60 % and 10 % passing, respectively. The results are presented in Figure 9. For both materials, Cu increases with applied stress, reflecting the progressive broadening of the particle size distribution induced by grain breakage. This increase is significantly more pronounced for carbonate sand, indicating a stronger degree of fragmentation and a higher production of fine particles.

At higher stress levels, the evolution of the uniformity coefficient tends to stabilize for both sands. This stabilization can be attributed to the establishment of a geometrically stable granular structure, in which the increasing number of contacts leads to a well-organized contact network (Hardin, 1985). Under these conditions, stress redistribution becomes more effective, reducing the likelihood of further particle breakage. This process is schematically depicted by Russell and Einav (2013), who showed how the progressive development of a stable contact network limits further fragmentation.

Overall, the evolution of the grain size distribution provides clear experimental evidence of particle fragmentation under increasing stress. The more pronounced and rapid shift of the GSD curves for carbonate sand confirms its higher susceptibility to

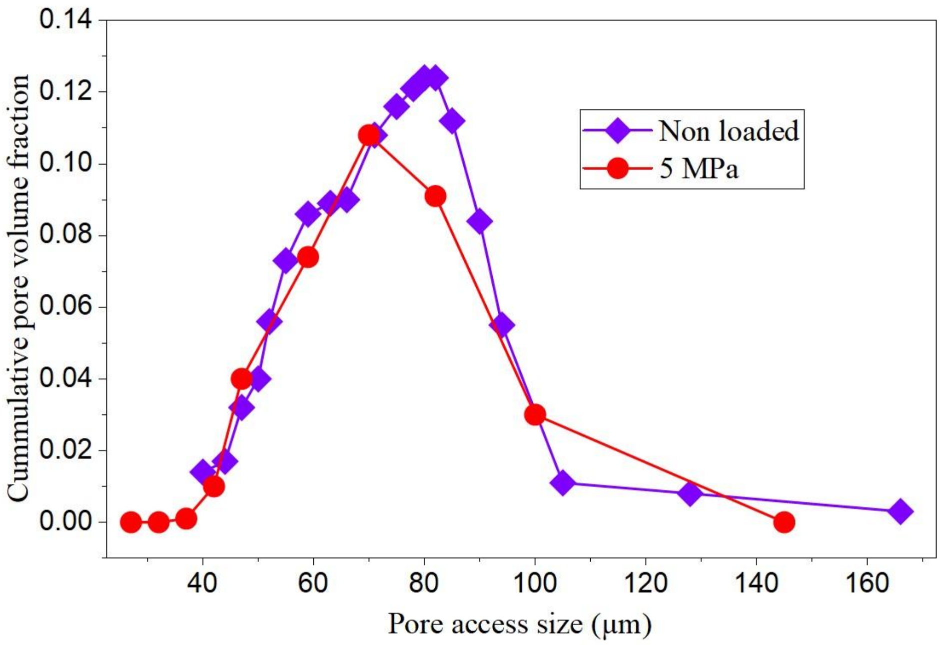

Fig. 10 Cumulative pore-access size distribution of the Hostun sand.

breakage, whereas the more gradual evolution observed for Hostun sand reflects its greater resistance to fragmentation. These results highlight the strong influence of material properties on the breakage process and its impact on the internal structure of granular assemblies.

3.3. *MICROSTRUCTURAL CHANGES AND EVOLUTION OF PORE SIZE DISTRIBUTION*

Loading granular materials such as sand under high stress levels induces significant modifications in their microstructure, including changes in grain size, interparticle contacts, porosity, pore size distribution, and specific surface area. These modifications primarily result from plastic deformation mechanisms involving grain rearrangement and/or grain breakage. To investigate the effects of applied stress on porosity and pore size distribution, both the tensiometric method and mercury intrusion porosimetry were employed on specimens subjected to different stress levels for both Hostun sand and carbonate sand.

For Hostun sand, the tensiometric method was applied at a stress level of 5 MPa, which is below the crushing threshold of 12.5 MPa. The results were compared with those obtained from a virgin sample (Fig. 10). At this stress level, no significant grain breakage is observed; instead, the deformation is mainly governed by grain rearrangement. This rearrangement leads to a reduction in pore size, reflected by a shift in the median pore size from approximately 75 μm to lower values, corresponding to a decrease of about 13 μm. In parallel, the porosity decreases by approximately 11 % compared to its initial value. This behavior indicates that, in the absence of particle breakage, microstructural changes are primarily controlled by densification through particle rearrangement and pore collapse.

Due to the fragility of the ceramic porous stone used in the tensiometric method, this technique is limited to relatively low stress levels. For carbonate sand, which exhibits a lower resistance to deformation, the tensiometric method was initially applied to characterize the pore size distribution in the uncompressed state. However, for applied stresses exceeding 10 MPa, the material develops sufficient cohesion, allowing mercury intrusion porosimetry to be used to assess the pore size distribution more accurately (Fig. 11).

The results presented in Figures 12 and 13 show a clear decrease in median pore size with increasing applied stress. This evolution is governed by two coupled mechanisms: grain rearrangement and grain

Fig. 11 Sample of Carbonate sand after an oedometric test at 30 MPa.

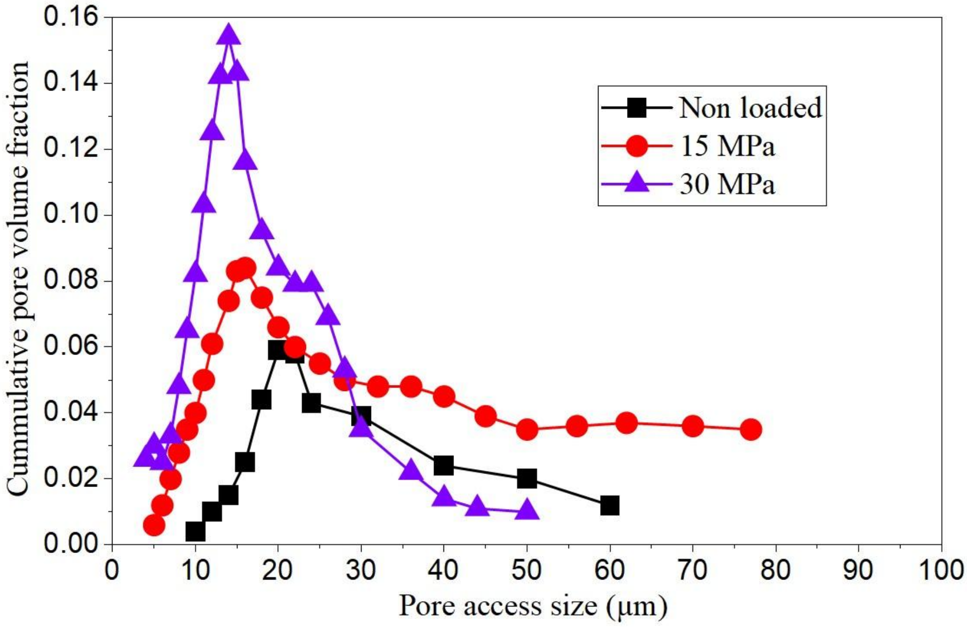

Fig. 12 Evolution of pore size distribution of Carbonate sand.

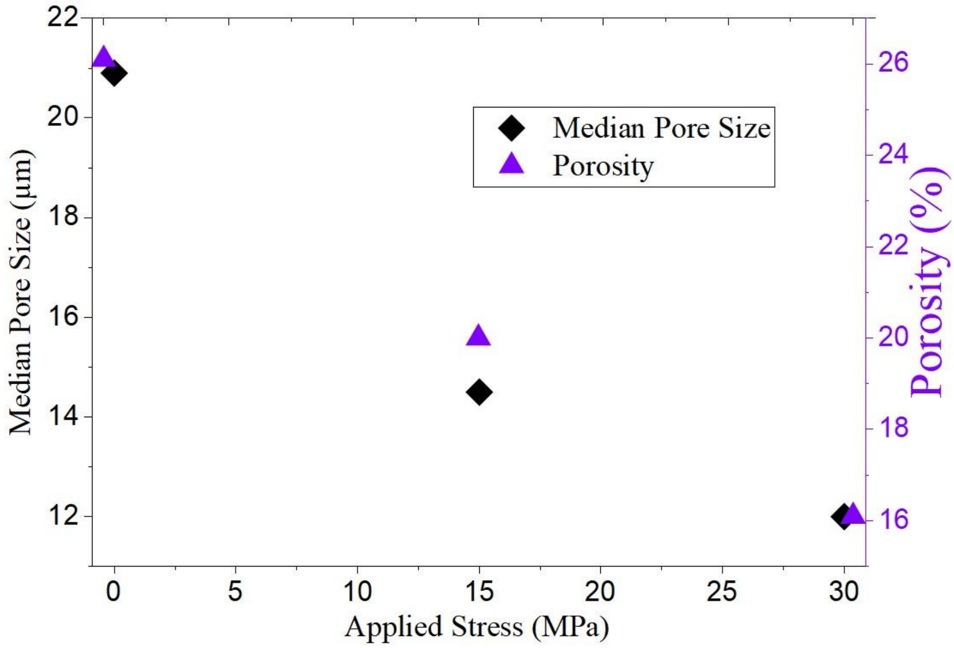

Fig. 13 Evolution of median pore size and porosity of Carbonate sand.

breakage. Grain rearrangement leads to a more compact packing structure and a reduction in the size of existing pores, while grain breakage generates fragments and fine particles that progressively fill the voids. The combined effect of these mechanisms results in a continuous reduction in pore size and a significant modification of the pore network.

For carbonate sand, this effect is particularly pronounced. The median pore size decreases from approximately 21 µm in the virgin state to 14.5 µm at 15 MPa and further to about 12 µm at 30 MPa. At the same time, the porosity decreases from an initial value of 0.26 to 0.20 at 15 MPa and to 0.16 at 30 MPa. These results demonstrate the strong impact of stress-induced microstructural changes on the internal structure of the material.

The reduction in pore size and porosity reflects the progressive densification of the granular assembly and the reorganization of the pore network. The generation of finer particles due to grain breakage enhances pore filling and reduces pore connectivity, leading to a more compact and mechanically stable structure. This evolution highlights the strong coupling between grain-scale processes and macroscopic behavior, where microstructural changes directly influence both the hydraulic and mechanical response of the material.

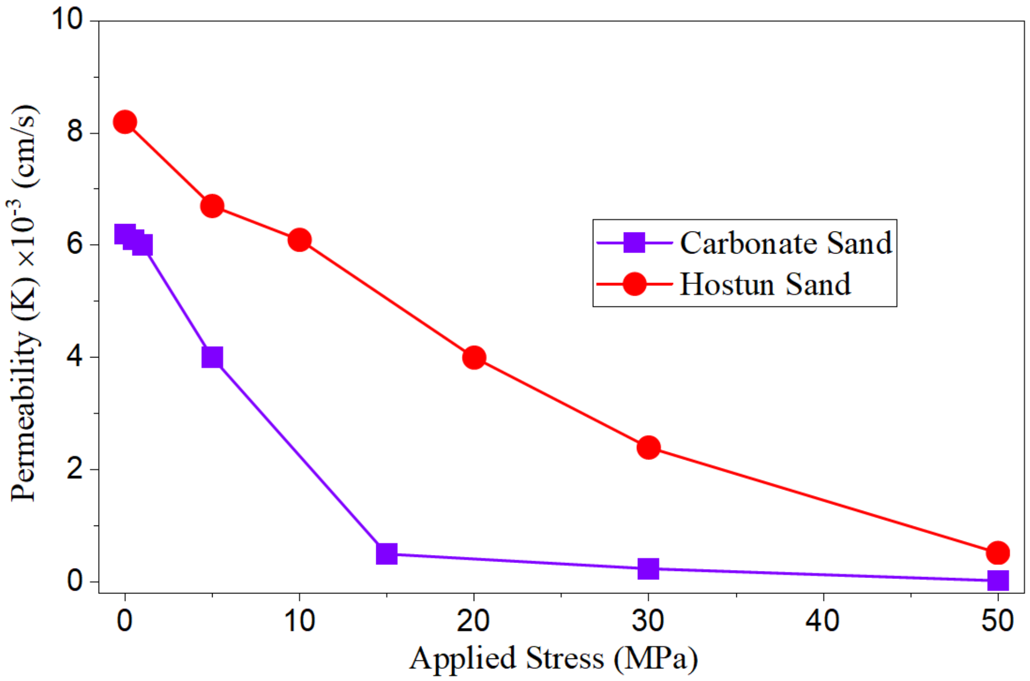

Fig. 14 Change in permeability under high stress.

3.4. PERMEABILITY EVOLUTION

High stress loading can significantly affect the hydraulic properties of granular materials, particularly permeability (Al-Hattamleh et al., 2013). In this study, permeability evolution under high stress was investigated using constant-head permeability measurements. The results, presented in Figure 14, show a significant decrease in permeability for both Hostun and carbonate sands as the applied stress increases.

A marked reduction in permeability is observed for both materials, with a more pronounced decrease in carbonate sand. This behavior is consistent with its higher susceptibility to deformation, characterized by more significant grain rearrangement, particle breakage, fines production, and overall densification.

The reduction in permeability can be explained by the combined effect of two primary mechanisms. First, grain rearrangement leads to pore collapse and a reorganization of the internal structure, resulting in a reduction of pore volume and connectivity. Second, grain breakage generates fine particles that progressively accumulate within the pore spaces. These fine particles partially fill and obstruct the pores, acting as barriers to fluid flow. As a result, the connectivity of the pore network is significantly reduced, which strongly limits water circulation within the granular medium. These underlying mechanisms, namely particle rearrangement leading to pore collapse and particle breakage, are further substantiated by both qualitative and quantitative observations obtained from three-dimensional X-ray tomography imaging, as reported in the studies of Karatza et al. (2017), Zhao et al. (2019) and Messioud et al. (2024).

The combined effect of pore collapse and pore clogging leads to a substantial modification of the pore structure, resulting in a drastic reduction in permeability. This evolution highlights the strong coupling between mechanical processes at the grain scale and the hydraulic behavior of the material. As the internal structure becomes denser and less connected, the material transitions toward a state characterized by reduced fluid transport capacity.

Overall, the results demonstrate that permeability evolution under high stress is primarily controlled by microstructural changes induced by grain rearrangement and particle breakage. The more pronounced decrease observed in carbonate sand reflects its higher crushability and greater production of fine particles, which intensify pore clogging and accelerate the loss of permeability.

4. MODELING

In this section, an attempt is made to model the experimental results presented above, with particular emphasis on the grain breakage process.

4.1. GRAIN BREAKAGE MODELING

Several models have been proposed in the literature to describe grain breakage under high stress levels. In this study, the Continuum Breakage Mechanics (CBM) framework developed by Einav (2007a, 2007b) is adopted. This model provides a thermodynamically consistent description of grain breakage by linking the evolution of the grain size distribution to energy dissipation mechanisms within the material.

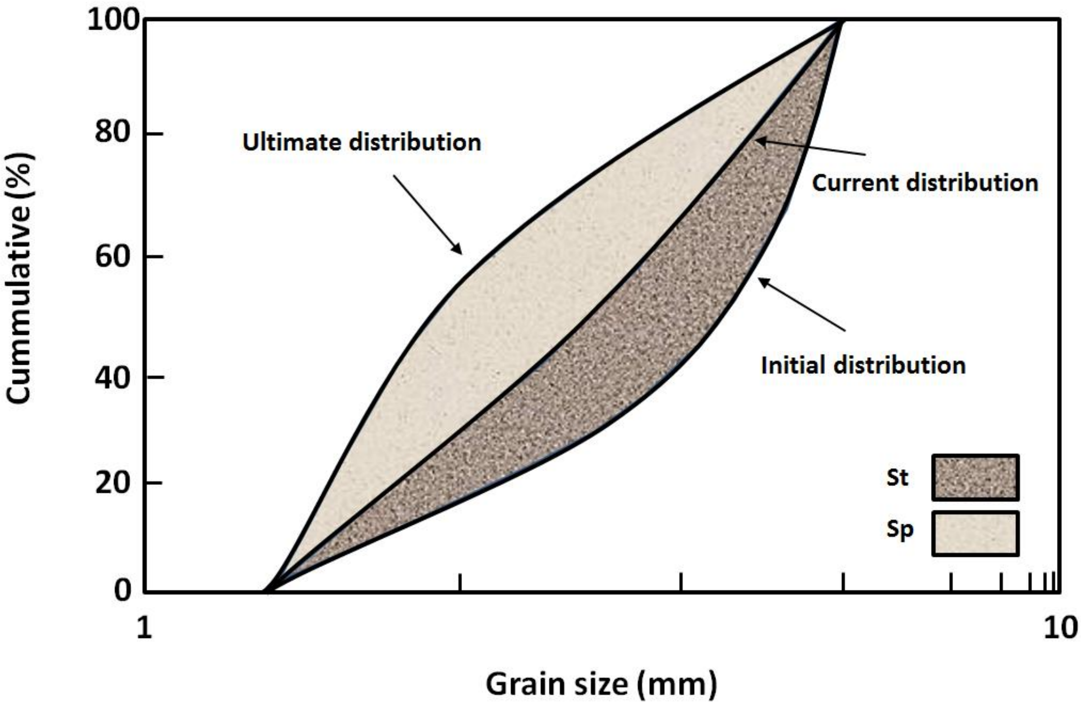

Fig. 15 Definition of the breakage index B (Einav, 2007a).

Within this framework, the evolution of grain breakage is quantified through a scalar variable, known as the breakage index B. This parameter is defined based on the evolution of the grain size distribution (GSD) curve during loading. Specifically, B represents the ratio between a partial area S_p, corresponding to the region between the current and initial GSD curves, and a total area S_t, defined as the region between the initial and ultimate GSD curves (Fig. 15). The breakage index is therefore expressed as:

$$B = \frac{S_p}{S_t} \tag{3}$$

where:

S_p is the partial area between the current and initial grain size distribution curves,

S_t is the total area between the initial and ultimate grain size distribution curves.

This definition allows the progressive evolution of particle breakage to be quantified in a normalized manner, with $B = 0$ corresponding to the initial state (no breakage) and $B = 1$ representing the ultimate breakage state.

The CBM model is based on an energy dissipation approach, in which the mechanical response of the granular assembly is governed by the balance between stored energy and dissipated energy during deformation. At the microstructural level, energy dissipation occurs mainly through two coupled mechanisms: grain crushing and interparticle frictional sliding and/or rotation. These mechanisms are intrinsically linked, as the activation of one promotes the development of the other (Einav, 2007b).

The yield surface of the CBM model is expressed as:

$$y \equiv \left(\sin(\omega)\frac{\psi_r(e_v^e)\vartheta}{\xi(e_v^e)(1-\vartheta B)}p\right)^2 + (\cos(\omega)\,E_B)^2 - \\ - G_B^2(1-B)^{-4} \le 0 \tag{4}$$

where ω is the plastic-breakage coupling angle, e_v^e is the elastic volumetric strain, ϑ is a statistical parameter measuring the proximity between the initial and final particle size distribution curves, $\psi_r(e_v^e)$ is the stored energy, B is the breakage factor, E_B is the residual breakage energy, and G_B is the strain energy constant of the material.

This formulation enables the coupling between mechanical loading and grain breakage to be captured within a unified framework. In particular, the model can be used to derive both the compressibility relationship $(e_v - p)$ (Strain - loading) and the evolution of breakage with stress $(B - p)$ (Breakage - Loading).

From this yield condition, the stress–breakage relationship can be expressed as:

$$p = p_{y0}\frac{(1-\vartheta B)}{\sqrt[2-m]{(1-B)^2}} \tag{5}$$

Where:

p is the applied stress,

p_{y0} is the initial crushing threshold,

m is a model parameter controlling the evolution of breakage with stress

This equation highlights the dependence of the applied stress on the degree of particle breakage and provides a direct link between the macroscopic mechanical response and the internal state of the

(a)

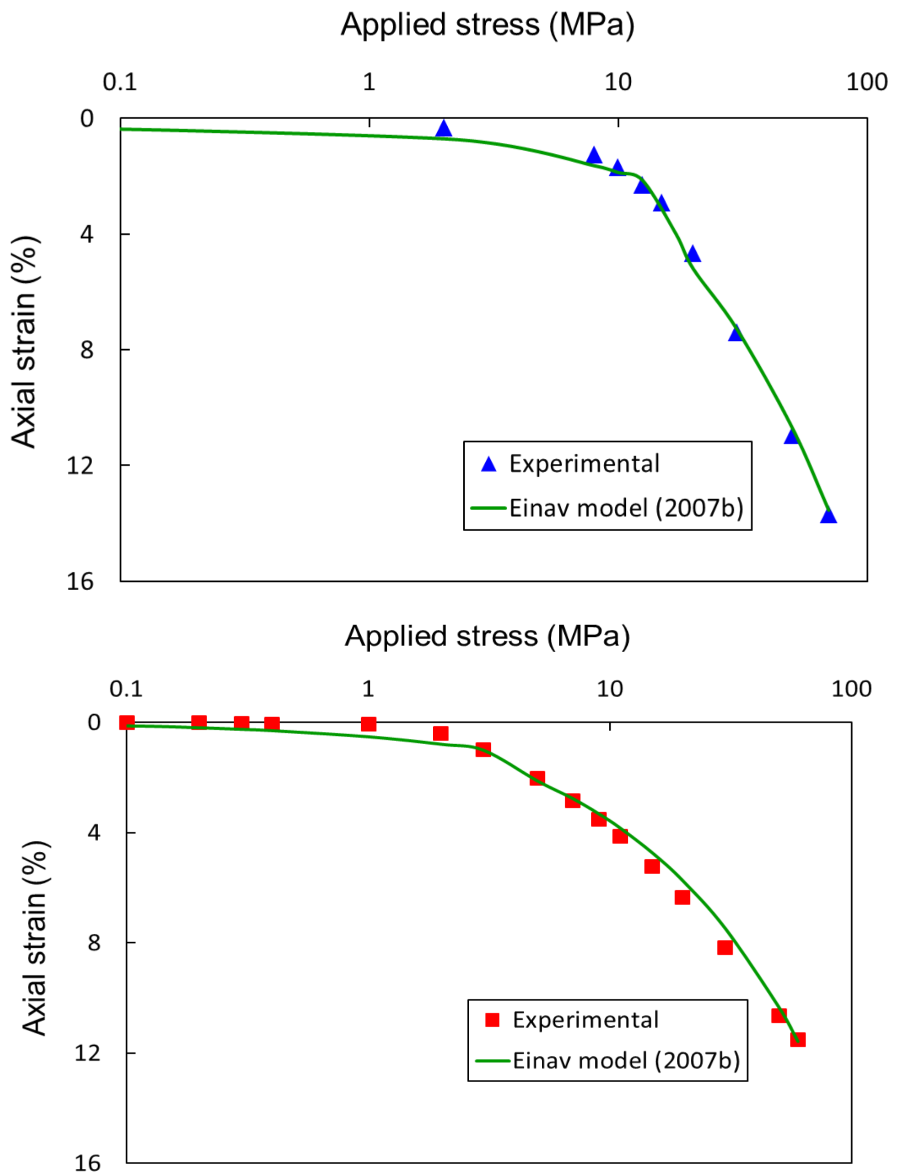

(b)

Fig. 16 Strain-stress ($e_v - p$) curves calibration of CBM model, (a) Hostun sand, (b) Carbonate sand.

material. As the breakage index increases, the material progressively evolves toward a more fragmented and denser structure, which is consistent with the experimental observations presented in the previous sections.

A comprehensive definition of all parameters, together with the full demonstration of the governing equations, is provided in detail in the works of Einav (2007a, 2007b).

4.2. MODEL CALIBRATION

The parameters of the CBM model were calibrated using the experimental results obtained for both sands. The strain-stress ($e_v - p$) curves are presented in Figure 16, while the breakage–stress ($B - p$) curves are shown in Figure 17. Here, e_v denotes the strain, p is the applied stress, and B is the breakage factor.

As shown in Figure 16, the CBM model provides a satisfactory representation of the experimental stress–strain response for both Hostun sand and carbonate sand. The model captures the main evolution of compressibility under increasing oedometric stress, including the progressive transition associated with particle breakage.

However, the prediction of the breakage–stress response ($B - p$) remains mainly qualitative. Although the CBM model reproduces the general trend of increasing breakage with stress, it does not accurately capture the experimental values of the breakage factor over the full stress range. This limitation is consistent with the observations reported by Einav (2007a).

The CBM model provides an accurate representation of the experimental stress–strain behavior. The corresponding calibrated parameters for both sand types are reported in Table 3.

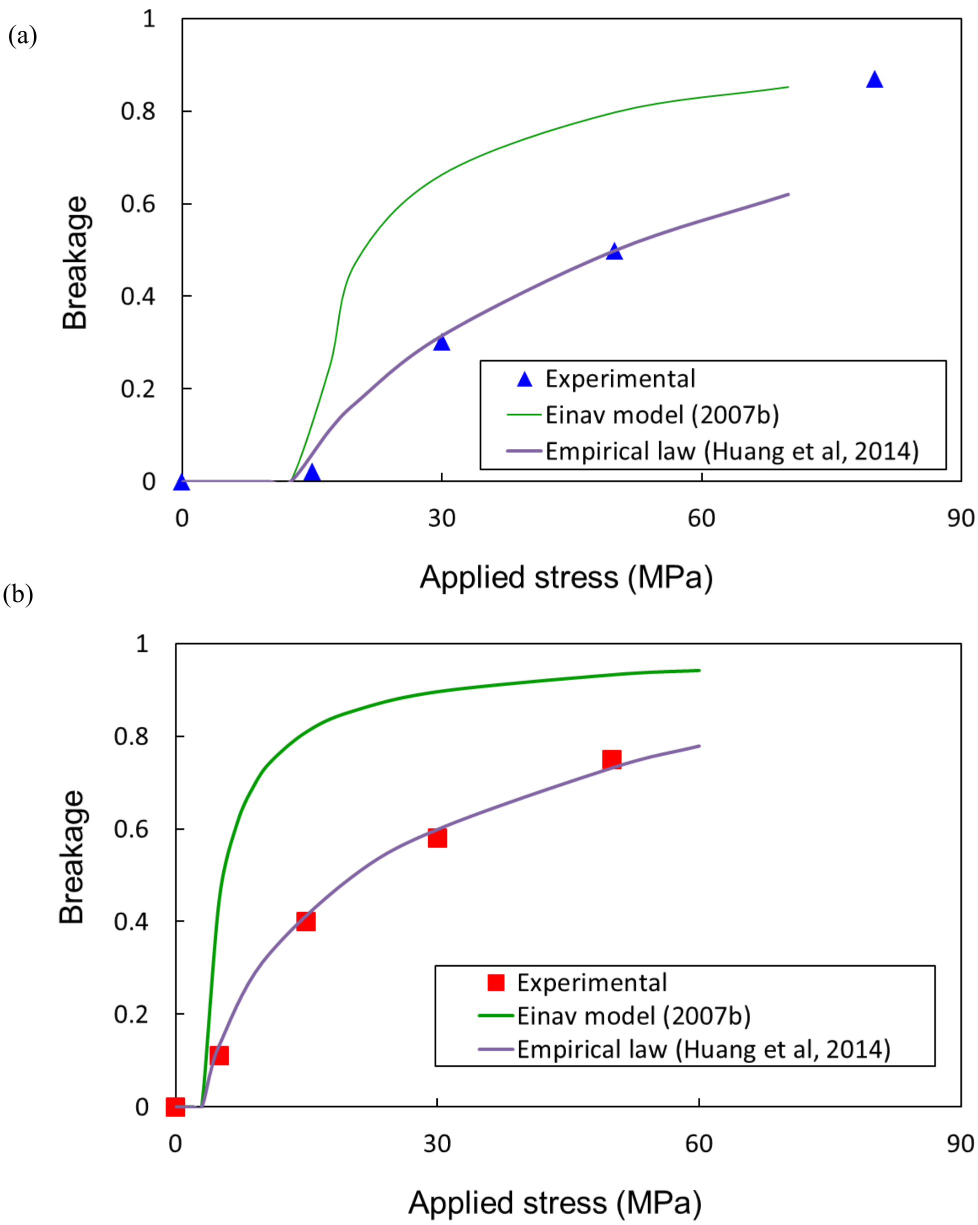

Fig. 17 Breakage-stress $(B - p)$ curves, (a) Hostun sand, (b) Carbonate sand.

Table 3 CBM model parameters for both types of sand.

	$G_B\ (kPa)$	ϑ	$K(kPa)$	$P_r\ (kPa)$	$\omega\ (°)$	m
Hostun sand	150	0.556	8500	1	71	0.47
Carbonate sand	14.51	0.457	7200	1	63	0.41

To improve the description of the experimental $(B - p)$ relationship, the empirical law proposed by Huang et al. (2014) was also considered:

$$B = \alpha ln\left(\frac{p}{p_{y0}}\right) \quad (6)$$

Where B is the breakage factor, p is the applied stress, p_{y0} is the crushing threshold (onset of particle breakage), and α is a model parameter controlling the rate of breakage evolution with stress. In this study, $\alpha = 0.36$ for Hostun sand and $\alpha = 0.26$ for carbonate sand.

As illustrated in Figure 17, this empirical relationship provides a better fit to the experimental breakage–stress curves for both materials. The comparison indicates that, while the CBM model is suitable for reproducing the overall stress–strain behavior, the empirical law more accurately captures the evolution of the breakage factor as a function of applied stress.

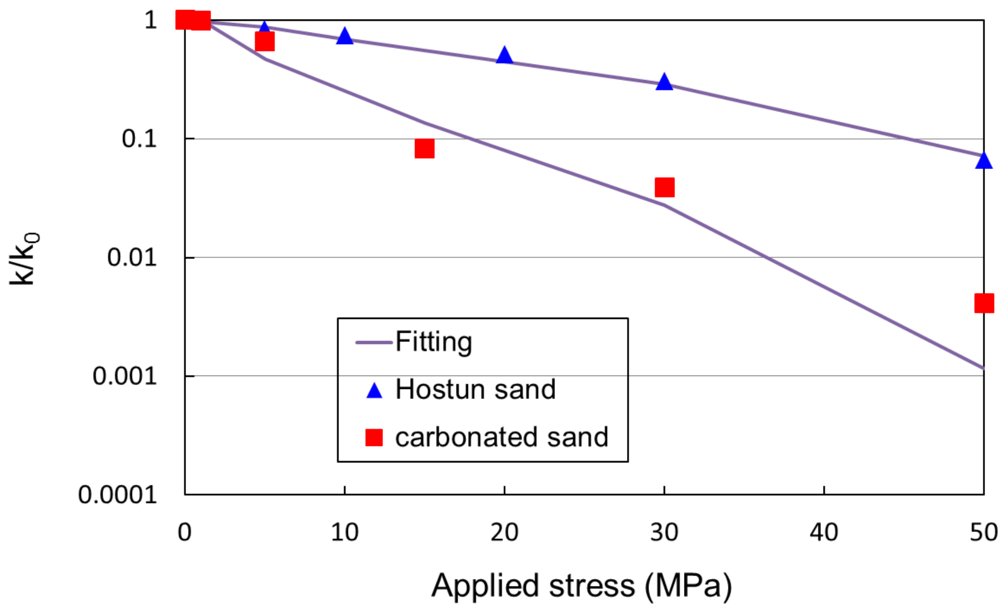

Fig. 18 Calibration of the permeability variation for the two sands using power low.

4.3. PERMEABILITY CHANGE

Several empirical relationships have been proposed in the literature to express permeability as a function of porosity, including the Kozeny–Carman equation and power-law formulations. In this study, the following power-law relationship is adopted:

$$\frac{K}{K_0} = \left(\frac{\phi}{\phi_0}\right)^n \tag{17}$$

Where K and K_0 are the permeability and initial permeability, respectively, ϕ and ϕ_0 are the porosity and initial porosity, respectively, and n is the power-law exponent.

The calibration of this relationship using the permeability measurements is presented in Figure 18. For Hostun sand, with an initial porosity of $\phi_0 = 0.42$, the calibrated exponent is $n = 9$. For carbonate sand, with an initial porosity of $\phi_0 = 0.26$, the calibrated exponent is $n = 9.16$. These values are in good agreement with the range reported in the literature for similar empirical relationships (David et al., 1994; Ghabezloo et al., 2009). The exponent n depends on the mechanisms controlling permeability reduction (Bernabé et al., 2003). The relatively high values obtained in this study highlight the significant influence of grain crushing on permeability evolution. Interestingly, nearly identical values of n are obtained for the two sands, despite their different mineralogical and granulometric characteristics, suggesting that grain breakage governs the permeability reduction mechanism in both cases.

The Einav (2007b) model was then used to estimate the relative contributions of grain breakage and grain rearrangement to porosity reduction through the coupling angle ω. This was achieved by setting $\omega = 0^{\circ}$, which corresponds to pure elastic breakage in the model, allowing the porosity reduction associated with grain breakage to be quantified. The porosity reduction due to grain rearrangement was then obtained by subtracting the breakage-induced porosity reduction from the total porosity reduction measured experimentally. The resulting porosity variations are presented in Figure 19.

The results show that grain breakage and grain rearrangement both contribute significantly to porosity reduction. Their contributions are of comparable magnitude, although the relative contribution of grain crushing increases with applied stress. This indicates that, at low stress levels, porosity reduction is mainly controlled by grain rearrangement and densification, whereas at higher stress levels, grain breakage becomes increasingly dominant.

Because grain rearrangement and grain crushing occur simultaneously during loading, their effects on permeability are coupled. To obtain an approximate estimation of their relative influence, it is assumed that grain rearrangement occurs before grain crushing. Under this assumption, the permeability change associated with grain rearrangement can be estimated using the power-law relationship and the porosity reduction due to rearrangement, $\Delta\phi_{re}$:

$$\frac{K_{re}}{K_0} = \left(\frac{\phi_0 - \Delta\phi_{re}}{\phi_0}\right)^n \tag{8}$$

Where K_{re} is the permeability associated with the porosity reduction caused by grain rearrangement, K_0 is the initial permeability, ϕ_0 is the initial porosity, $\Delta\phi_{re}$ is the porosity reduction due to grain rearrangement, and n is the power-law exponent defined above.

The calculated permeability changes due to grain rearrangement, together with the total permeability reduction obtained experimentally, are shown in

(a)

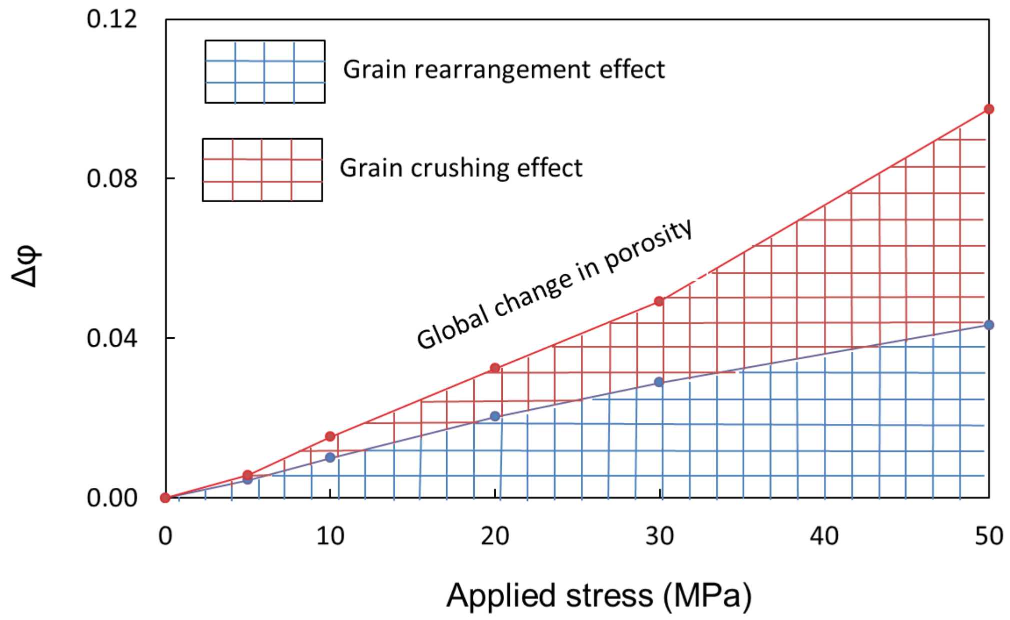

(b)

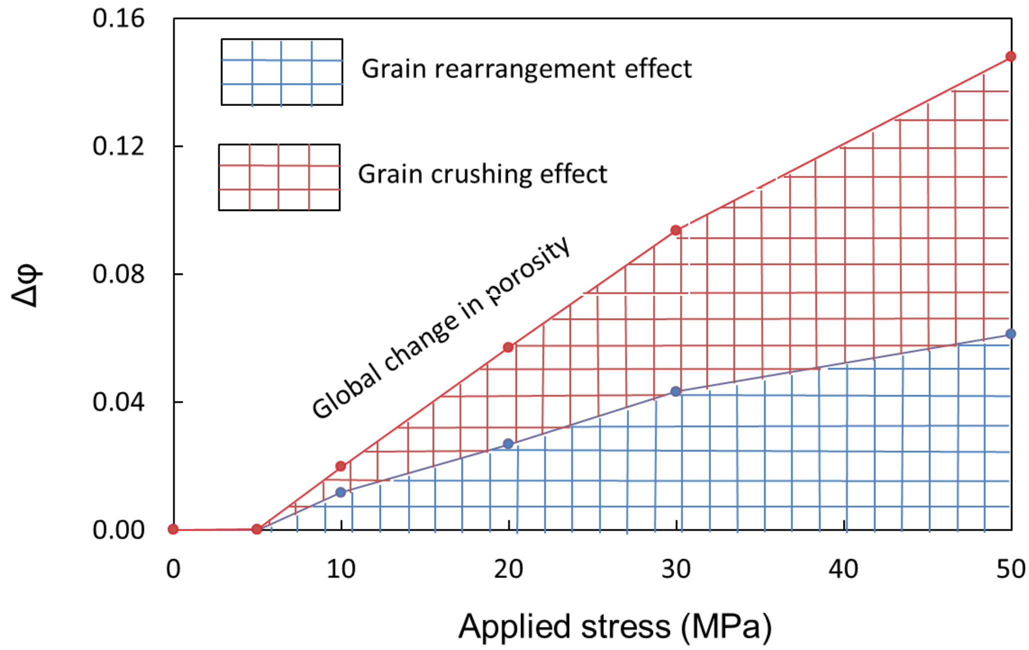

Fig. 19 Change in porosity due to the two studied phenomena (a) Hostun sand, (b) Carbonate sand.

Figure 20. The results indicate that grain rearrangement and grain crushing both influence permeability reduction, but their relative roles evolve with stress level. Similar to porosity evolution, grain rearrangement contributes significantly at lower stress levels, while the contribution of grain crushing becomes increasingly important as stress increases.

This effect is more pronounced for carbonate sand than for Hostun sand. The stronger permeability reduction observed in carbonate sand is associated with its higher susceptibility to grain breakage, which generates finer particles and promotes pore filling and pore-network constriction. Consequently, the connectivity of the pore structure is more strongly reduced, leading to a larger decrease in permeability. Overall, the results show that permeability evolution under high stress is governed by the coupled effects of grain rearrangement, grain crushing, and the associated changes in porosity and pore connectivity.

5. CONCLUSION

This study investigated the effects of grain breakage on the mechanical response, grain size distribution, pore-access size distribution, porosity, and permeability of two sands with contrasting mineralogical properties, namely Hostun silica sand and carbonate sand, subjected to high oedometric stresses. The experimental results were combined with grain breakage modeling and permeability–porosity analysis to clarify the coupled role of particle rearrangement and grain crushing in controlling the hydro-mechanical behavior of granular materials under high stress conditions.

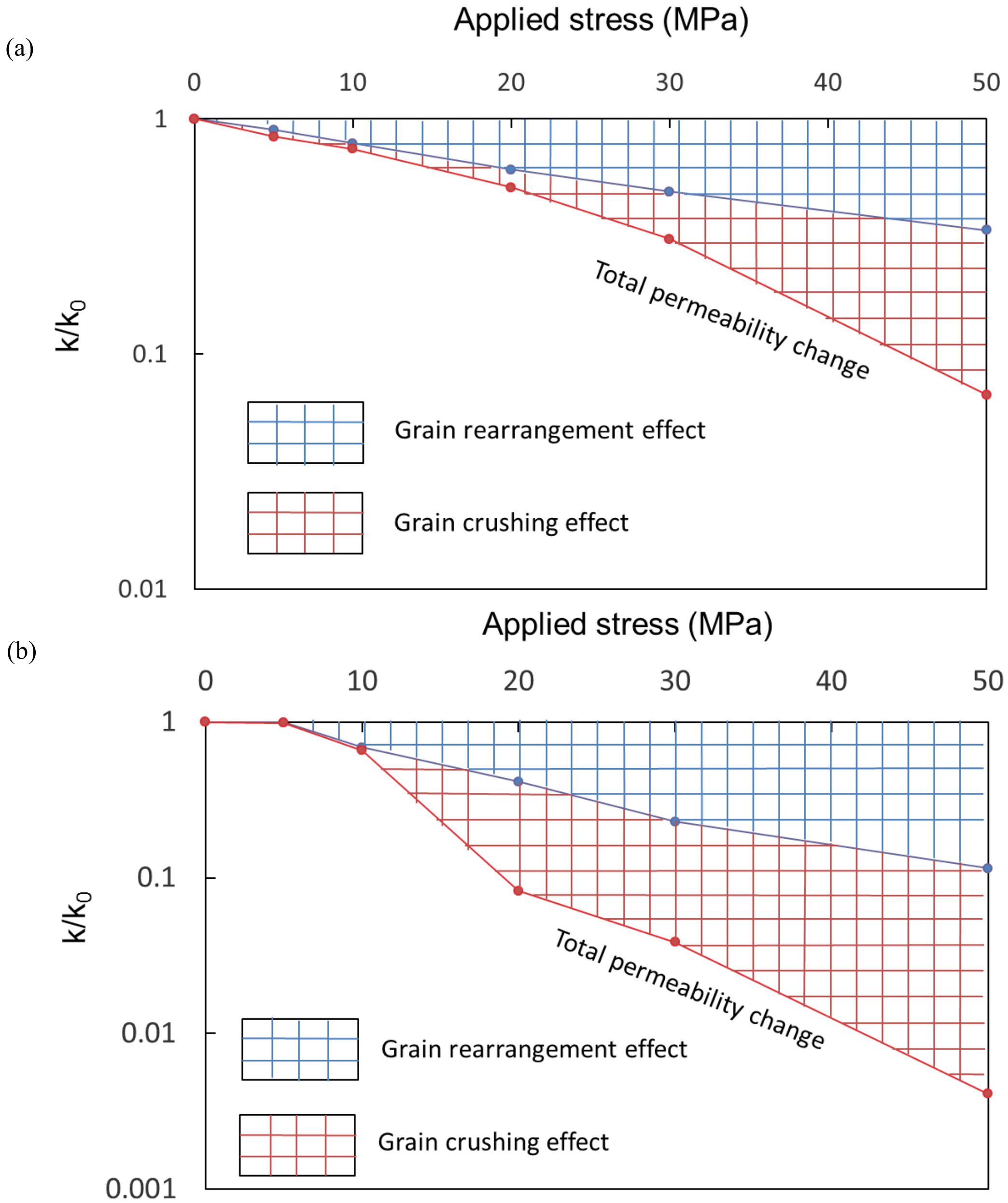

Fig. 20 Change in permeability due to the two studied phenomena (a) Hostun sand, (b) Carbonate sand.

The main findings can be summarized as follows:

- The stress–strain curves showed a clear change in slope associated with the onset of particle breakage, with a crushing threshold of about 12.5 MPa for Hostun sand and about 3 MPa for carbonate sand.
- Increasing stress caused a progressive shift of the grain size distribution toward finer particles, indicating continuous particle fragmentation and evolution toward an ultimate grading state.
- Carbonate sand exhibited earlier and more pronounced grain breakage than Hostun sand, reflecting its higher crushability and lower resistance under oedometric loading.
- The pore-access size distribution and porosity decreased with increasing stress. This reduction was governed by two coupled mechanisms: grain rearrangement, which causes pore collapse, and grain breakage, which generates fragments and fine particles that progressively fill the voids.
- Permeability decreased significantly with increasing stress for both sands, with a stronger reduction for carbonate sand. This behavior is mainly attributed to pore structure modification, pore clogging by fine particles, and reduced pore connectivity.
- The CBM framework provided a satisfactory representation of the stress–strain response, while the empirical breakage–stress relationship better reproduced the evolution of the breakage factor with applied stress.
- The power-law relationship between permeability and porosity showed that grain rearrangement and

grain breakage both contribute to permeability reduction, with the influence of grain breakage becoming more significant at higher stress levels.

Overall, the results highlight the strong coupling between grain breakage, pore structure evolution, and permeability reduction in sands subjected to high stress conditions. The comparative analysis of Hostun and carbonate sands shows that mineralogical composition and breakage resistance strongly influence the hydro-mechanical response. These findings provide useful experimental and modeling insights for predicting the behavior of crushable granular materials in geotechnical, geomechanical, and petroleum reservoir engineering applications.

DECLARATION OF COMPETING INTEREST

The authors have no relevant financial or non-financial interests to disclose.

DATA AVAILABILITY

All data are available upon reasonable request from the corresponding author.

REFERENCES

Al-Hattamleh, O.H., Al-Deeky, H.H. and Akhtar, M.N.: 2013, The Consequence of Particle Crushing in Engineering Properties of Granular Materials. Int. J. Geosci., 4, 7, 1055–1060. DOI: 10.4236/ijg.2013.47099

Altuhafi, F., Jardine, R.J., Georgiannou, V.N. and Sim, W.W.: 2017, Effects of particle breakage and stress reversal on the behaviour of sand around displacement piles. Geotechnique, 68, 6, 1–10. DOI: 10.1680/jgeot.17.P.117

Asaf, Z., Rubinstein, D. and Shmulevich, I.: 2007, Determination of discrete element model parameters required for soil tillage. Soil Tillage Res., 92, 1–2, 227–242. DOI: 10.1016/j.still.2006.03.006

Aung, K.K., Rahardjo, H., Leong, E.C. and Toll, D.G.: 2001, Relationship between porosimetry measurement and soil–water characteristic curve for an unsaturated residual soil. Geotech. Geol. Eng., 19, 3–4, 401–416. DOI: 10.1023/A:1013125600962

Benammar, C., Feia, S., Khechai, A., Denine, S. and Della, N.: 2025, Grain breakage in shear bands and its effect on the permeability decrease of granular material specimens during triaxial loading. Acta Geodyn. Geomater., 22, 3, 317–322. DOI: 10.13168/AGG.2025.022

Bernabé, Y., Mok, U. and Evans, B.: 2003, Permeability-porosity relationships in rocks subjected to various evolution processes. Pure Appl. Geophys., 160, 5, 937–960. DOI: 10.1007/PL00012574

Biarez, J. and Hicher, P.Y.: 1994, Elementary Mechanics of Soil Behaviour. Rotterdam: A.A. Balkema.

Burdine, N.T.: 1953, Relative permeability calculations from pore size distribution data. J. Pet. Technol., 5, 3, 71–78. DOI: 10.2118/225-G

Buscarnera, G. and Einav, I.: 2021, The mechanics of brittle granular materials with coevolving grain size and shape. Proc. R. Soc. A: Math. Phys. Eng. Sci., 477, 2246, 20201005. DOI: 10.1098/rspa.2020.1005

Coop, M.R., Sorensen, K.K., Bodas Freitas, T. and Georgoutsos, G.: 2004, Particle breakage during shearing of a carbonate sand. Geotechnique, 54, 3, 157–163. DOI: 10.1680/geot.2004.54.3.157

David, C., Wong, T.F., Zhu, W. and Zhang, J.: 1994, Laboratory measurement of compaction-induced permeability change in porous rocks: Implications for the generation and maintenance of pore pressure excess in the crust. Pure Appl. Geophys., 143, 1–3, 425–456. DOI: 10.1007/BF00874337

Dong, Z., Cheng, Y.P., Tong, C., Liu, H. and Zhang, Y.: 2024, DEM modelling of particle crushing of single carbonate sand using the improved bonded particle model. Powder Technol., 432, 118599. DOI: 10.1016/j.powtec.2023.118599

Einav, I.: 2007a, Breakage mechanics—Part I: Theory. J. Mech. Phys. Solids, 55, 6, 1274–1297. DOI: 10.1016/j.jmps.2006.11.003

Einav, I.: 2007b, Breakage mechanics—Part II: Modelling granular materials. J. Mech. Phys. Solids, 55, 6, 1298–1320. DOI: 10.1016/j.jmps.2006.11.004

Feia, S., Dupla, J.-C., Canou, J., Ghabezloo, S., Sulem, J., Chabot, B., Aubry, E. and Mainguy, M.: 2017, An experimental setup with radial injection for investigation of transport and deposition of suspended particles in porous media. Geotech. Test. J., 40, 6, 1115–1124. DOI: 10.1520/GTJ20160032

Feia, S., Ghabezloo, S., Bruchon, J.-F., Sulem, J., Canou, J. and Dupla, J.-C.: 2014, Experimental evaluation of the pore-access size distribution of sands. Geotech. Test. J., 37, 4, 613–620. DOI: 10.1520/GTJ20130126

Feia, S., Sulem, J., Canou, J., Ghabezloo, S. and Clain, X.: 2016, Changes in permeability of sand during triaxial loading: effect of fine particles production. Acta Geotech., 11, 1, 1–19. DOI: 10.1007/s11440-014-0351-y

Fredlund, M.D., Fredlund, D.G. and Wilson, G.W.: 2000, An equation to represent grain-size distribution. Can. Geotech. J., 37, 4, 817–827. DOI: 10.1139/t00-015

Frossard, E., Hu, W., Dano, C. and Hicher, P.-Y.: 2012, Influence of grain properties and water content on the mechanical behaviour of granular materials. Granul. Matter, 14, 4, 449–463. DOI: 10.1007/s10035-012-0355-8

Fukumoto, T.: 1990, A grading equation for decomposed granite soil. Soils Found., 30, 1, 27–34. DOI: 10.3208/sandf1972.30.27

Fukumoto, T.: 1992, Particle breakage characteristics of granular soils. Soils Found., 32, 1, 26–40. DOI: 10.3208/sandf1972.32.26

Ghabezloo, S., Sulem, J. and Saint-Marc, J.: 2009, Evaluation of a permeability-porosity relationship in a low-permeability creeping material using a single transient test. International J. Rock Mech. Min. Sci., 46, 4, 761–768. DOI: 10.1016/j.ijrmms.2008.10.003

Han, C., Vanapalli, S.K. and Li, Q.: 2016, Effect of moisture content on particle breakage of a granular base material. Geotech. Lett., 6, 1, 1–6. DOI: 10.1680/jgele.15.00112

Hardin, B.O.: 1985, Crushing of Soil Particles. J. Geotech. Eng., 111, 10, 1177–1192. DOI: 10.1061/(ASCE)0733-9410(1985)111:10(1177)

Huang, J.Y., Xu, S.L. and Hu, S.S.: 2014, Influence of particle breakage on the dynamic compression responses of brittle granular materials. Mech. Mater., 68, 15–28. DOI: 10.1016/j.mechmat.2013.08.002

Charlaix, E. and Ciccotti, M.: 2009, Capillary condensation in confined media. Spec. Top. Granular Phys., 121–142. https://arxiv.org/abs/0910.4626

Chen, Q., Li, Z., Dai, Z., Wang, X., Zhang, C. and Zhang, X.: 2023, Mechanical behavior and particle crushing of irregular granular material under high pressure using discrete element method. Sci. Rep., 13, 8233. DOI: 10.1038/s41598-023-35022-w

Chen, Y., Yu, B., Zhang, K., Zhang, M., Xu, G. and Chen, Z.: 2018, Permeability evolution and particle size distribution of saturated crushed sandstone under compression. Geofluids, 043420, 1–12. DOI: 10.1155/2018/6043420

Chuhan, F.A., Kjeldstad, A., Bjørlykke, K. and Høeg, K.: 2002, Porosity loss in sand by grain crushing—Experimental evidence and relevance to reservoir quality. Mar. Pet. Geol., 19, 1, 39–53. DOI: 10.1016/S0264-8172(01)00049-6

Igwe, O., Sassa, K. and Wang, F.W.: 2007, The influence of grading on the shear strength of loose sands in stress-controlled ring shear tests. Landslides, 4, 1, 43–51. DOI: 10.1007/s10346-006-0051-2

Juang, C.-H. and Holtz, R.D.: 1986, Fabric, pore size distribution, and permeability of sandy soils. J. Geotech. Eng., 112, 9, 855–868. DOI: 10.1061/(ASCE)0733-9410(1986)112:9(855)

Karatza, Z., Andò, E., Papanicolopulos, S.A., Ooi, J. and Viggiani, G.: 2018, Evolution of deformation and breakage in sand studied using X-ray tomography. Geotechnique, 68, 2, 107–117. DOI: 10.1680/jgeot.16.P.208

Karatza, Z., Andò, E., Papanicolopulos, S.-A., Viggiani, G. and Ooi, J.Y.: 2017, Evolution of particle breakage studied using x-ray tomography and the discrete element method. EPJ Web of Conferences, 140, 07013. DOI: 10.1051/epjconf/201714007013

Karatza, Z., Andò, E., Papanicolopulos, S.A., Viggiani, G. and Ooi, J.Y.: 2019, Effect of particle morphology and contacts on particle breakage in a granular assembly studied using X-ray tomography. Granul. Matter, 21, 44. DOI: 10.1007/s10035-019-0898-2

Katz, A.J. and Thompson, A.H.: 1986, Quantitative prediction of permeability in porous rock. Phys. Rev. B, 34, 11, 8179–8181. DOI: 10.1103/PhysRevB.34.8179

Lee, K.L. and Farhoomand, I.: 1967, Compressibility and Crushing of Granular Soil in Anisotropic Triaxial Compression. Can. Geotech. J., 4, 1, 68–86. DOI: 10.1139/t67-012

Marachi, N.D.: 1969, Strength and deformation characteristics of rockfill materials (PhD thesis). Department of Civil Engineering, University of California, Berkeley.

Marcial, D., Delage, P. and Cui, Y.J.: 2002, On the high stress compression of bentonites. Can. Geotech. J., 39, 1, 1–9. DOI: 10.1139/t01-071

McDowell, G.R.: 2002, On the yielding and plastic compression of sand. Soils McDowell.

Messioud, S.E., Dadda, A., Feia, S. et al.: 2024, Effect of Particle Breakage of Sand Under High Oedometric Stress on its Microstructural Properties Using 3D X-ray Micro-tomography. Indian Geotech. J., 54, 2379–2395. DOI: 10.1007/s40098-024-00879-9

Nakata, Y., Hyodo, M., Hyde, A.F.L., Kato, Y. and Murata, H.: 2001, Microscopic particle crushing of sand subjected to high pressure one-dimensional compression. Soils Found., 41, 1, 69–82. DOI: 10.3208/sandf.41.69

Novello, E.A. and Johnston, I.W.: 1989, Normally consolidated behaviour of geotechnical materials. In Proceedings of the 12th International Conference on Soil Mechanics and Foundation Engineering, 3, 2095–2100. Rio de Janeiro, Brazil: International Society for Soil Mechanics and Foundation Engineering.

Russell, A.R. and Einav, I.: 2013, Energy dissipation from particulate systems undergoing a single particle crushing event. Granul. Matter, 15, 3, 299–314. DOI: 10.1007/s10035-013-0408-x

Tengattini, A., Das, A. and Einav, I.: 2016, A constitutive modelling framework predicting critical state in sand undergoing crushing and dilation. Geotechnique, 66, 9, 695–710. DOI: 10.1680/jgeot.14.P.164

Tong, X., Chen, Q. et al.: 2019, A stochastic particle breakage model for granular soils subjected to one-dimensional compression with emphasis on the evolution of coordination number. Comput. Geotech., 112, 72–85. DOI: 10.1016/j.compgeo.2019.04.010

Turcotte, D. L.: 1986, Fractals and fragmentation. J. Geophys. Res., Solid Earth, 91(B2), 1921–1926. DOI: 10.1029/JB091iB02p01921

Wang, F.W., Sassa, K. and Wang, G.H.: 2002, Mechanism of a long-runout landslide triggered by the August 1998 heavy rainfall in Fukushima Prefecture, Japan. Eng. Geol., 63, (1–2), 169–185. DOI: 10.1016/S0013-7952(01)00080-1

Xiao, Y.: 2022, Evolution of particle shape produced by sand breakage. Int. J. Geomech., 22, 5, 04022041. DOI: 10.1061/(ASCE)GM.1943-5622.0002333

Yamamuro, J.A. and Lade, P.V.: 1996, Drained sand behavior in axisymmetric tests at high pressures. J. Geotech. Eng., 122, 2, 109–119. DOI: 10.1061/(ASCE)0733-9410(1996)122:2(109)

Yao, L., Chen, J., Xiao, Y. and Peng, Y.: 2025, Granular soil particle breakage prediction model based on population evolution theory. Sci. Rep., 15, 13161. DOI: 10.1038/s41598-025-92057-x

Zhang, C., Einav, I. and Nguyen, G.: 2013, The end-bearing capacity of piles penetrating into crushable soils. Geotechnique, 63, No. 5, 341–354. DOI: 10.1680/geot.11.P.117

Zhang, J., Li, Y. and Wang, R.: 2021, A generalized plastic model for gravelly soils considering evolution of void ratio and particle breakage. Front. Phys., 9, 767821. DOI: 10.3389/fphy.2021.767821

Zhao, B., Wang, J., Andò, E., Viggiani, G. and Coop. M.R.: 2019, An investigation of particle breakage under one-dimensional compression of sand using X-ray micro-tomography. Can. Geotech. J., 57, 5, 754–762. DOI: 10.1139/cgj-2018-0548